SEIPIN PROMOTES LIPID DROPLET BIOGENESIS

APPROVED BY SUPERVISORY COMMITTEE

JOSEPH ALBANESI

JOEL GOODMAN

JOACHIM SEEMANN

JIN YE

SEIPIN PROMOTES LIPID DROPLET BIOGENESIS

by

CHRISTOPHER LEE HILTON

DISSERTATION

Presented to the Faculty of the Graduate School of Biomedical Sciences

The University of Texas Southwestern Medical Center

In Partial Fulfillment of the Requirements

For the Degree of

DOCTOR OF PHILOSOPHY

The University of Texas Southwestern Medical Center

Dallas, Texas

August, 2012

DEDICATION

I would like to thank the members of my Graduate Committee, Dr. Joel Goodman- my mentor, my fellow lab members-past and present, Drs. Tallquist and Ravnik for help in my application to this institution, and my family and friends for their love and support..

SEIPIN PROMOTES LIPID DROPLET BIOGENESIS

CHRISTOPHER LEE HILTON, Ph.D.
The University of Texas Southwestern Medical Center, 2012

JOEL GOODMAN, Ph.D.

Seipin is an ER membrane protein that is required for adipogenesis in mammalians. Humans lacking functional seipin have virtually no visible adipose tissue. Seipin has been shown to be essential for the later stages of the adipogenic program in mouse pre-adipocytes. In yeast, the absence of seipin (Fld1p) leads to clusters of tiny lipid droplets or "supersized" ones, suggesting a role of the protein in droplet formation. To determine if this is true we created yeast strains that allowed us to "turn on" lipid droplet synthesis by the regulated expression of enzymes that create either triacylglycerol (TAG) or sterol ester (SE), the main neutral lipid components of droplets, in a droplet-null background with seipin (*4KO*) or without it (*4KOfld1Δ*). Using fluorescence microscopy, I showed that the number of newly formed TAG fluorescent bodies (individual droplets or clusters of unresolvable small droplets) decreased but their size increased in the absence of seipin. The large fluorescent bodies in *4KOfld1Δ* were fluorescently dimmer and had an irregular perimeter compared to those in the 4KO strain, while

their intracellular membranes stained with BODIPY had brighter fluorescence, suggesting that seipin is involved in the packaging of TAG. Electron microscopy showed that the TAG fluorescent bodies were clusters of small droplets. Levels of whole-cell TAG were generally similar during droplet formation, although somewhat lower at early time points. Seipin deletion had a milder effect on formation of SE fluorescent bodies. We conclude that seipin plays a direct role in normal lipid droplet assembly. Finally, in several side projects, I leaned about a possible role of seipin in droplet protein composition, the effects of different detergents on the seipin homo-oligomer, and the lack of a role of seipin in ER stress.

TABLE OF CONTENTS

LIST OF TABLES

LIST OF FIGURES

LIST OF APPENDICES

LIST OF DEFINITIONS

LD – Lipid droplet

FB – Fluorescent body

TAG – Triacylglycerol

SE – Steryl-ester

DAG-Diacylglycerol

PA – Phosphatidic acid

IGF1 – Insulin-like growth factor 1

PPAR – Peroxisome proliferator-activated receptor

HDEL – Peptide corresponding to the C-terminus of yeast BiP

ADRP – PLIN2: Adipose differentiation-related protein

aP2 – Adipocyte protein 2

GLUT4 – Glucose transporter type 4

C/EBP – CCAAT-enhancer-binding protein

HAC1 – Homologous to Atf/Creb1 (transcription factor that activates UPR when spliced)

FITC – Fluorescin isothiocyanate

CHAPS – 3-[(3-cholamidopropyl)dimethylammonio]-1-propanesulfonate

DTT – Dithiothreitol, reducing agent

MEF – Mouse embryonic fibroblast

IBMX – 3-isobutyl-1-methylxanthine, a competitive nonselective phosphodiesterase inhibitor

Introduction

My research is focused on the role that seipin, the product of *FLD1* in the yeast *Saccharomyces cerevisiae*, has in lipid droplet biogenesis. My lab identified yeast seipin in a lipid droplet morphology screen of a gene knockout library [2]. Seipin is orthologous to the product of *BSCL2* (Berardinelli-Seip congenital lipodystrophy type 2) in humans. Mutation of *BSCL2* or knockout of the analogous genes in mice or flies results in lipodystrophy, or lack of normal adipose tissue. My introduction will focus on a brief history of Berardinelli-Seip congenital lipodystrophy, current knowledge of seipin, and current models and questions of lipid droplet biogenesis.

A. Berardinelli- Seip Congenital Lipodystrophy

BSCL2 was first identified in humans as the second locus of mutations for the congenital disease Berardinelli- Seip lipodystrophy [3]. BSCL2 lipodystrophy is an autosomal recessive disorder, and most of the mutations identified in patients are thought to be null mutations or to produce inactive protein. Its prevalence is only 1 in 10,000,000 people in the United States, but it is much more common in Lebanon and Portugal with prevalence of 1 in 200,000 and 1 in 500,000 respectively [4]. (As a reference point, Severe Combined Immunodeficiency, or "bubble boy disease", has a prevalence of 1:100,000-1:50,000 [5], with about half

of the cases caused by various autosomal recessive mutations [6].) Lipodystrophy, of which BSCL2 is the most severe form in humans, can be caused by external factors such as HIV infection [7, 8], antiretroviral drugs [7], or repeated injections of insulin or other drugs [9-12], or by hereditary factors, such as mutations in lamin A/C or in 1-acyl-sn-glycerol-3-phosphate acyltransferase beta (AGPAT2), causing BSCL type 1. Most milder lipodystrophies present as abnormal deposits of fat, but BSCL2 is a practically complete loss of adipose tissue, including mechanical adipose in and around joints and cushioning the soles of the feet [13].

The virtual absence of adipose tissue leads to other symptoms of the disease. Without the ability to store neutral lipids normally, the body stores fat ectopically in liver, muscle, and other tissues, and in the bloodstream. Storing lipids in the liver and spillover into the blood leads to early-onset diabetes mellitus, as it does in many obese individuals. Also common to insulin resistance [14], is acanthosis nigricans, characterized by dark velvety folds of the skin. This is thought to be a result of insulin spillover into the skin [14, 15]. As the liver accumulates fat, it can expand in size (hepatomegaly) enough to result in pain. This can occur in other organs too, such as the spleen. Enlargement of organs in the abdominal region can lead to umbilical hernias. Loss of adipocytes leads to underproduction of leptin and adiponectin[16]. Hypermetabolic characteristics are often seen in lipodystrophic individuals, including an increase in appetite, linear growth, and bone age [4]. While leptin deficiency probably contributes to the

increase in appetite, accelerated linear growth [17, 18] and bone age [19, 20] may have as much to do with the ability of insulin to activate IGF1 receptors at high concentrations [21]. *BSCL2* loss of function probably relates to the mental retardation seen in many sufferers, since *BSCL2* is highly expressed in human brain, although the cause of mental retardation is understudied [3]. Van Maldergem *et al*. stated that MRI was normal in mentally challenged BSCL2 lipodystrophy patients, but no data was shown or citation offered [22]. Lastly, a decrease in plasma HDL is seen in all lipodystrophies, including BSCL2 [23].

Several of the effects in the patients with BSCL2 are seen in any disorder where pre-pubertal diabetes is a hallmark, including acromegaloid features, muscle hypertrophy, and many of the problems seen with the female reproductive system. The features of acromegaly associated with BSCL2 are the enlargement of the hands, feet, and jaw, and they are linked to diabetes independent of IGF-1 [24]. Muscle hypertrophy is probably caused by both juvenile diabetes through IGF-1 signaling [25] and by ectopic neutral lipid storage [26]. Female reproductive problems of BSCL2 include hirsutism (facial or chest hair), menstrual irregularities and, in the worse cases, polycystic ovarian syndrome. All three of these can result from insulin stimulation of IGF-1 receptors in ovaries resulting in androgen production [14, 27]. In fact, acromegaly, organomegaly, a hypermetabolic state, and muscle hypertrophy may all be secondary to increased IGF-1 signaling in BSCL2 lipodystrophy.

BSCL2 mutations also have effects on lifespan. One study showed premature death in BSCL2 lipodystrophy to be as high as 15% [22]. Premature death can result from diabetes-related renal failure [22], liver failure [22] resulting from cirrhosis [26], hypertrophic cardiomyopathy [22] (in 20-30% of BSLC2 lipodystrophy presentations), and acute pancreatitis and pancreatic failure (when unmanaged) resulting from high circulated lipid levels [28, 29]. Hypertrophic cardiomyopathy is another symptom of BSL2 lipodystrophy that may be caused by increased IGF-1 signaling [14].

Management of BSLC2 lipodystrophy is limited to treating diabetes and hyperlipidemia in all BSCL2 individuals, and care of the more severe symptoms of cardiomyopathy and mental retardation as they occur. Extreme reduction of fat intake, one of the most effective ways to manage this severe disorder [30], helps reverse the hyperlipidemia, and the limitation of saturated fats and cholesterol improves risk of heart disease. The fibric acid class of PPARα agonists and ω-3 fatty acids (fish oils) also improve hypertriglyceridemia [30]. The complications of lipodystrophy due to childhood diabetes are treated with insulin. Metformin can be used to help insulin sensitivity and curb appetite [31]. The PPARγ agonist troglitazone appeared to improve two patients in clinical trials, even though it did not promote adipocyte differentiation. (Early experiments with cultured cells showed that seipin knockdown decreased PPARγ activity, and a PPARγ agonist promoted adipocyte differentiation in cells in which seipin was knocked-down [32].)

A very beneficial treatment of BSCL2 lipodystrophy, particularly to attenuate appetite and metabolic disorder, is leptin replacement [33, 34], although leptin replacement has led to renal failure and T-cell lymphoma [33]. Management of the hypertrophic cardiomyopathy usually involve β-blockers [35], anti-arrhythmia medicine [36] (if arrhythmia is present), and if severe, myectomy [37] or implanted pacemakers [38]. Management of intellectual impairment includes special education, speech therapy, and vocational training as needed. Better understanding of the causes of the manifestations of the disease and the mechanism of the function of seipin could lead to better therapies that would improve these peoples' lives and possibly those suffering from insulin resistance. If the onset of diabetes could be delayed, several of the IGF-1-related presentations of BSCL2 lipodystrophy might be avoided.

A clue to seipin function might be provided by consideration of the other loci mutated in generalized lipodystrophy. The most closely related to BSCL2 in terms of disease phenotype is BSCL type 1, caused by mutations in AGPAT2, as noted above. The enzyme converts lysophosphatidic acid into phosphatidic acid (PA) by adding an acyl chain to the glycerol backbone. Subsequent dephosphorylation of PA, and addition of a third acyl chain results in triacylglycerol (triacylglyceride), one of the two major lipid families in lipid droplets (the other being steryl-esters). BSCL1 is a less severe disorder than BSCL2 since mechanical fat develops [13], mental retardation does not occur, and

leptin levels are slightly higher [13, 4]. This implies that seipin may be upstream of AGPAT2 before a branch-point in the genetic pathway, although BSCL1 has an additional phenotype of lytic bone lesions [39]. It is important to note that seipin itself has no homology to any enzymatic domains; human and rodent seipin, however, have weak homology to midasin, a nuclear chaperone required for ribosome maturation [40].

Other causes of congenital generalized lipodystrophy are mutations in caveolin-1 (one case) and cavin-1 (multiple cases [41, 42]), which allows caveolin-1 to form oligomers and deform the membrane to produce caveolae [43, 44]. The lipodystrophy caused by caveolin-1 loss-of-function spared bone marrow fat and had a less severe loss of mechanical fat compared to BSCL2 [45]. Additionally, there was no mental retardation or acromegaly, although the caveolin-1 deficient patient had mild hypocalcemia. Caveolin-1 deletion in mice also resulted in lipodystrophy [46]. Cavin-1 loss-of-function lipodystrophy (also called CGL4) is similar to caveolin-1 lipodystrophy in adipose tissue development, but it is further characterized by smooth muscle hypertrophy, skeletal myopathy, impaired bone development, and heart arrhythmias that vary in type between individuals [41, 42, 47]. Cavin-1 mutations in muscle biopsies or cultured cells cause caveolin 1, 2, and 3 to appear less punctate and even absent at plasma membrane, determined by immunohistology, and caveolae were also difficult to detect. The pleotropic

effects of cavin mutations could explain why there were more defects in the corresponding patients compared to the one with caveolin-1 deletion.

B. Seipin

Identification

In 2001, Magre *et al.* first mapped thirteen mutations responsible for congenital generalized lipodystrophy to a locus with an unidentified open reading frame that they termed *BSCL2* and a gene product that they termed seipin after the co-discoverer of the syndrome [3]. Nine mutations coded for nonsense mutations resulting in protein truncations, three were large deletions, and one was a missense mutation. While heterogeneity was evident, they all were assumed to be loss-of-function alleles. (The authors assumed the A212P missense substitution led to altered protein folding.) In this report, they also mapped mutations in patients from twenty families to *AGPAT2*, a previously identified locus for congenital, generalized lipodystrophy, furthering the idea that multiple loci were responsible for the loss of adipose tissue in human development. Finally, they identified homologues to *BSCL2* in mice and flies, and they showed that brain and testis were the tissues that had the highest expression of seipin mRNA transcripts in humans.

Twenty years later, the field has yet to identify the molecular function of seipin. In one sense, we have *only* had two decades to study the function of this gene, and the field is just now studying knockout mice to determine the function of the gene in the context of lipodystrophy. In another sense, the seipin field has *already* had two decades to study this gene in detail, and while multiple phenotypes have been described, no one has deduced function. I believe progress towards identifying function has been made, as discussed in the following section, although this goal has not yet been achieved.

Topology and Structure

After seipin was discovered, some effort was made to determine its membrane topology and intracellular location. Before linkage to human seipin was discovered, yeast seipin was included in a study of thirty-seven uncharacterized yeast proteins that were predicted, based on primary sequence and likely secondary structure, to contain two transmembrane domains [48]. To assess topology, the authors fused either the asparagine-linked glycosylation motive (active in the ER lumen) and a His4p domain (conferring histidine prototrophy if facing the cytosol) to the carboxy termini of the proteins. They concluded from this study that the carboxy terminus, and by inference the amino terminus, of the proteins were both exposed in the cytosol [48].

A subsequent report assessed the topology of human seipin, specifically the long 462 amino acid isoform 1 (see below for multiple products). From expression *in vivo*, the human protein was found by Windpassinger *et al.* to be glycosylated in the sequence, termed the loop, between the two predicted transmembrane domains [49]. Lundin *et al.* used *in vivo* expression and *in vitro* reconstitution to confirm this and show that the protein was not glycosylated when the site was mutated [50]. This indicates that the loop has access to the lumen of the secretory pathway, consistent with a previous report of ER localization from a paper on glycosylation mutants of seipin [49]. When Lundin *et al.* engineered versions of seipin with glycosylation sites in the N- or C-termini, neither was glycosylated, indicating that they were facing the cytosol [50]. Therefore, the parts of the protein are now referred to as N-tail (facing the cytosol), N-transmembrane domain (NTM), lumenal loop, C-transmembrane domain (CTM), and C-tail (also facing the cytosol) (Figure 1 [50]). One of the interesting findings of this paper was that the lumenal loop had one weak scoring transmembrane domain (Figure 2 [50]), suggesting that the loop is somewhat hydrophobic, and unpublished data from our lab shows that the luminal loop expressed separately and targeted to the ER lumen is tightly associated with the ER membrane.

As previously stated, the first human seipin paper identified mouse and fruit fly homologues of human *BSCL2*, and since then, frog, worm, rat, yeast, several plant, and other seipins have been identified. All of these share secondary

structure, especially the transmembrane domains and several sections of the intervening loop that form secondary structure, as shown in Figure 3 [2]. While the core is conserved, species-specific functions and/or interactions, assuming they exist, may occur outside of this area in the N-tail and C-tail extensions, which vary in length (4-102aa, and 4-467aa, respectively) and sequence [51].

Expression

Human seipin has two isoforms, at least in cell culture. Isoform 1 (462 amino acids total) contains an 89 amino-acid-long N-tail and a 138 amino-acid-long C-tail, while the loop contains 194 amino acids and each transmembrane domain contains 21 amino acids. Isoform 2 (398 amino acids) contains a shortened 25 amino acid N-tail, but the rest of the protein is identical to isoform 1. There are three human transcript variants shown by northern blotting in the Magre *et al.* paper that produce these isoforms, two of which were confirmed by Windpassinger *et al.* [49]. Transcript one is 2.2 Kb and transcript two is 1.8 Kb, starting at two different sites in exon 1 [49]. The entire gene codes eleven exons, with transmembrane domains coding from exons 2 and 7. While transcript two is specifically expressed in the brain and transcript one is nearly ubiquitous, both can produce either isoform. There is a third transcript in the Magre *et al.* paper that is about 1.6 Kb and starts in exon 2. This short transcript presumably just produces isoform 2 [50], and it was also ubiquitously expressed [3]. If cDNA is

expressed *in vivo*, it produces both isoforms, yet if it is expressed *in vitro*, only the longer isoform 1 is produced [50]. Additionally, when both isoforms are produced, the larger isoform is more abundant. The yeast protein contains 285 amino acids with slightly longer predicted transmembrane domains than in human seipin, each of 23 amino acids, and a slightly longer loop domain of 218 amino acids compared to human seipin. The N- and C-tails are both markedly shorter than human seipin, 12 and 11 amino acids, respectively.

In the Magre *et al.* paper [3], human seipin mRNA was mostly expressed in the brain and testis. Subsequent work using a human seipin (hseipin) antibody revealed brain expression in motor neurons in the spinal cord and cortical neurons of the frontal lobe, while in the testis, spermatid were stained, peaking at developmental steps 6 and 7 [52]. In contrast, there was considerably less mRNA expression in (in descending order) the pancreas, kidney, ovary, skeletal muscle, liver, heart, adipose tissue, colon, and small intestine [3]. It is interesting that expression in adipose tissue, where seipin appears to have a critical function, is very low. Conversely, it is somewhat surprising that testis expression is so high, since male sterility is not a phenotype of BSCL2. High expression in the brain makes some sense, since mental retardation is a fairly common feature of BSCL2, and mutations in glycosylation of seipin lead to the autosomal dominant disorders in the nervous system termed seipinopathies (discussed below).

In contrast, in mice and flies, adipose tissue had the highest or second-highest expression among tissues examined [53-55]. Testis had the highest expression in mice, roughly equal to adipose, yet brain expression is considerably lower, and is similar to that in the kidney [53, 54]. In the fly, brain had the lowest level of expression of those tissues they measured [55]. Possibly, seipin is required for specialized uses of fat, such as the myelin sheath of motor neurons, rather than the bulk storage of fat. In mice, for example, seipin was expressed at a higher level in brown adipose tissue than white. Regardless of these differences, expression patterns should be clues to seipin function that the field has not yet decoded.

Seipinopathies

Seipinopathies are a group of neurodegenerative diseases related to an impairment of the myelin sheath [56] that are caused by autosomal dominant mutations in *BSCL2*. They are often considered gain of function mutations, while BSCL2 lipodystrophy is caused by loss of function mutations. Seipinopathies were first described by Windpassinger in the role of *BSCL2* in distal hereditary motor neuropathy and Silver syndrome [49]. Aside from mostly confirming the work from Magre in tissue expression and showing that expressed seipin localized to the ER, Windpassinger *et al*. showed that *BSCL2* was the locus of mutation for these two neurological diseases [49]. The mutations were single amino acid substitutions that abolished asparagine-linked glycosylation. Lack of

glycosylation seemed to cause seipin to form large aggregates, which they believed was the cause of neurodegeneration. This thread of thought was continued by Ito and Suzuki. Mutant seipin was probably unfolded in the ER since it could be pulled down in an immunoprecipitation with the ER chaperone calnexin. Expression of mutant seipin caused an increase in protein expression of ER stress proteins in a neural cell line [57]. Mutant seipin also increased tunnel staining in non-neural cells, indicating that it caused apoptosis and suggesting that the neurodegeneration was due to cell death caused by ER stress.

Yagi and Suzuki released contradictory evidence, however, when they published the phenotype of mice expressing mutant seipin. While the animals had upregulated ER stress markers, similar to what they found earlier in cells, there was no increase in neuronal death [58]. These data indicate that ER stress is associated with (they state sufficient for) seipinopathies, but nerve degeneration appears not to be caused neural death. Most recently, evidence was published that the aggregates were actually protective [59]. They attenuated ER stress (measuring the protein CHOP) and cell death (assayed by terminal deoxynucleotidyl transferase dUTP nick-end labeling) when aggregates were present compared to cells that were expressing mutant seipin and did not have aggregates (now termed inclusion bodies). Considering all these data, the model is now that the inclusion bodies segregate mutant seipin from wild type seipin. Perhaps the neurons that cannot efficiently do this have decreased function.

In summary, while seipinopathies first appeared to be a result of nonspecific aggregation of unglycosylated seipin, current insight suggests that neurological manifestations in patients may be due to a specific dominant-negative effect related to the inclusion bodies themselves, or seipin specifically. The dominant-negative effect of mutant seipin may sequester wild type seipin to inclusion bodies, resulting in a loss of wild type seipin function in cells with inclusion bodies. The inclusion bodies may protect from cell death, but either dominant-negative effects or inclusion bodies may impair myelin formation and neurotransmission.

Yeast seipin (Fld1p) discovery and its role in lipid droplet (LD) morphology

As mentioned before, our lab identified yeast seipin, although the gene name FLD1 (Fewer Lipid Droplets) was given to it slightly later [60]. The name is somewhat of a misnomer because, while *fld1Δ* droplets appear fewer than wild type by fluorescence microscopy, this is not always true when observed by electron microscopy. Lipid droplets in *fld1Δ* yeast generally fall into two morphologies: large droplets ("supersized"), or small droplets in clusters, although clusters can appear in fluorescence microscopy to be large, irregular (in shape) droplets. Considering this heterogeneity, not all seipin knockout cells have fewer droplets than wild type. Electron microscopy reveals that clusters are comprised of numerous small lipid droplets with electron dense inclusions that

appear to be chaotically budding from ER membranes, much like what is seen in fibroblasts and lymphoblasts from BSCL2 patients [2, 61]. Supersized droplets are seen more often when yeast are grown in minimal medium to the stationary phase of growth. This seems to be due to an increase in phosphatidic acid, since PA is elevated in these cells and supplementing with inositol (which reduces PA) greatly diminishes the percentage of cells with supersized droplets [62]. It has also been suggested that supersized droplets are a result of smaller ones fusing, since this has been shown to occur *in vitro* [60]. In this paper, Wolinski *et al*. also demonstrated the reversibility of the formation of supersized droplets by adding fresh rich media to *fld1Δ* yeast, which favors a small droplet cluster phenotype [63], indicating that they have the ability to undergo fission as well.

Our group reported that clusters of small droplets are often wrapped by membranes, the result of local ER proliferation [2]. This has been confirmed by Wolinski *et al*., who additionally showed that, supersized droplets are in close proximity to "a bar-like proliferation of the ER," and "a fraction of LD (small droplets)…was almost completely enclosed by ER membranes [63]." They proposed that these tangles may be the cause of the impairment that they observed in LD inheritance and intracellular movement in *fld1Δ* yeast compared to wild type. In contrast to direct *fld1Δ* phenotypes, ER wrapping, LD clustering, and supersized droplets may all be compensatory mechanisms to reduce lipolysis. (Recent evidence indicates that lipolysis is upregulated in BSCL2-/- mice, which will be

discussed below [64].) Indeed, Wolinski *et al*. observed a decrease in Tgl3p localization to LD [63]. They interpreted this as a defect due to *fld1Δ*, but it could be an indirect effect of ER proliferation masking the droplet surface. Droplet proliferation can also be caused by ER stress. However, we have evidence (discussed in Results) that seipin deletion and the resulting cluster formation does not cause an ER stress response in yeast.

The **clustering** of small, aberrant droplets and/or supersized droplet phenotypes may be yeast-specific, since neither are present in fibroblasts or lymphoblasts from BSCL2 patients. If seipin has crucial control over an enzyme related to PA utilization in yeast (and therefore droplet size), the pathway of PA utilization may be redundant in humans. In *BSCL2*-/- mice, hepatic tissue has oversized multilocular lipid droplets [64, 65]. The increase in size is probably simply due to excess lipidemia and lipid uptake. However, mouse embryonic fibroblasts from *BSCL2*-/- mice that are differentiated into adipocytes appear to have larger, fewer droplets during differentiation (Day 5 to Day 10) compared to those from the wild type controls. Therefore, in tissues that can make large droplets, seipin deletion appears to make supersized droplets in mammalian cells as well as yeast. The actual clustering of the small chaotic lipid droplets in tangles present in *fld1Δ* yeast has so far only been seen in yeast.

Seipin oligomerization

While over-expressed in cultured cells, seipin localizes widely in the ER, but it specifically localizes to ER-lipid droplet junctions as puncta when the chromosomal copy is viewed as a mCherry fusion protein in yeast [2]. In transmission electron microscopy images, seipin localized by immuno-gold staining was also concentrated at ER-lipid droplet associations. When the fusion protein is over-expressed on a low-copy plasmid, large patches rather than puncta are observed. Droplets are always associated with endogenously expressed seipin-mCherry under basal conditions, but if droplets are induced to increase in size by adding oleic acid, the seipin puncta outnumber droplets (Adeyo and Goodman, unpublished data). This may indicate that seipin is involved in droplet birth, but not droplet expansion. Our evidence that seipin is at this junction suggests that it is important for this ER-droplet communication. However, since cells still make droplets in the absence of seipin, it is not required for lipid droplet biogenesis.

Droplet-ER communication appears to be important since most of the droplets appear to be associated with the ER in yeast. To co-localize droplets and the ER, we expressed CFP-HDEL as an ER marker, and used BODIPY, a fluorescent dye that binds to neutral lipid, to mark lipid droplets. Virtually all lipid droplets (95%+) remained associated with ER. Time-lapse microscopy showed that droplets could move laterally on the ER plane, which they often did, but no dissociation from the ER membrane was observed [66], a result that has been independently confirmed [63].

Discrete seipin puncta suggest that seipin protein may self-associate, or at least localize to ER micro-domains. This hypothesis is aided by the fact that seipin expression is fairly low (about 800 molecules per cell compared to 17700 molecules/cell of Sec63p, another ER membrane protein [67]), but it is still visible by fluorescence microscopy at endogenous levels in these puncta. Additionally, immuno-gold transmission electron microscopy revealed seipin concentrated at LD-ER junctions although it is also seen in other places in the ER. During a study aiming to find binding partners, we found that seipin indeed oligomerizes [68]. Detergent-solubilized seipin from crude membranes migrates on detergent glycerol gradients during centrifugation faster than predicted if it were a monomer. After correcting for detergent molecules using H2O and D2O sucrose gradients, both over-expressed seipin-mCherry, endogenous (genome level) seipin-13xmyc fusion proteins, and over-expressed, untagged seipin migrate at a velocity in sucrose gradients consistent with a homo-oligomer of 9 molecules [68]. This rules out the effect of a specific epitope tag, any tag at all, or overexpression (at least between the two fusion proteins) causing oligomerization. The fact that the expression level does not change the degree of oligomerization is evidence for the stability of this nonamer.

The only way to alter the size of the oligomer was to over-express seipin-mCherry in cells expressing normal seipin-13xmyc at the genome level; this shifted the migration of seipin-13xmyc to a larger apparent molecular weight [66].

Nearly all the mutations that cause lipodystrophy in humans are nonsense or frameshift mutations in the lumenal loop domain, resulting in truncated proteins that are assumed to be either non-functional in the context of adipose formation, or quickly degraded. One missense mutation towards the end of the lumenal loop domain, A212P (numbered by isoform 2), causes the formation of an aberrant but full-length protein [2]. Our lab generated the homologous mutation in yeast, G225P [2].

We showed, using an antipeptide antibody we developed, that [G225P]seipin is much less abundant than wild type form suggesting it is quickly degraded [68]. A C-terminal epitope tag increases the stability of [G225P]seipin. Upon arrest of protein synthesis, [G225P]seipin almost completely degrades within six hours while wild type hardly changes its. While we could detect untagged over-expressed [G225P]seipin in concentrated cell extracts with our antibody, we were unable to detect it after centrifugation to try to assess its oligomerized form [68]. However, we could sufficiently detect over-expressed [G225P]seipin-mCherry or [G225P]seipin-13xmyc expressed chromosomally (from its endogenous promoter). Using these proteins and wild type controls, we found that both -mCherry and -13xmyc versions still formed oligomers, although they were reduced to a trimer and hexamer, respectively [68]. Therefore, it was not surprising that addition of over-expressing [G225P]seipin-mCherry decreased the oligomeric size of genome-level [wt]seipin-13xmyc oligomer present in

membrane preparations between the sizes of the oligomers produced by the two proteins separately. This implies that seipin self-associates, and that [G225P]seipin stabilized by C-terminal tags, has a dominant effect on the size of oligomer. The point mutation in the loop does not change the structure of the protein enough (while tagged) to discourage seipin-seipin interactions. It will be interesting to see what parts of the protein can and cannot associate.

One caveat to these studies is the possibility that these oligomers are not exclusively seipin molecules, and there have been several attempts in our laboratory to find other binding proteins to seipin. Several proteins were found to co-migrate in glycerol gradients with seipin, and mass spectroscopic analysis identified some of these to be mitochondrial ATPase subunits. However, the ATPase is a similar size as the seipin nonamer. Pull-down studies did not reveal ans specific binding proteins other than common chaperones (Binns and Goodman, unpublished data). To more definitively identify any binding partners, we purified seipin from solubilized crude membranes using a 13xmyc tag version of seipin with an engineered TEV site between the protein and tag. After binding the protein to anti-myc beads, we separated seipin from the tag with TEV protease [68]. When this preparation was run on SDS-PAGE and silver-stained, seipin was the major band; minor bands of protein were also detectable, but they were also seen in parallel extracts from cells not expressing seipin. While we are still limited by the detection level of silver stain and cannot rule out unstable

interactions with seipin (monomer or oligomer), thus far we have been unable to detect any heterologous binding partners for seipin using these approaches.

To determin if the seipin nonamer macromolecule had visible structure, purified seipin was subjected to negative staining and electron microscopy. We saw multiple disk shaped particles that appeared to have holes in the center (like toroids) [68]. We assume this is the structure of the oligomer, since monomers might be too small to be visible. There is a discrepancy in that the Stokes' radius we calculated for seipin (with the 13xmyc) was about twice the actual radius of the toroids [68]. However, Stokes' radius was calculated from data using the 13xmyc tag, while the toroids had the epitope tag removed before electron microscopy imaging. The myc epitope is only 10 amino acids, but in the toroid, 13xmyc would add an additional 1170 amino acids compared to 2565 amino acids of seipin (both assuming a seipin homo-nonamer). That is not enough to account for the doubling in radius of the complex, but 13xmyc could be more splayed out compared to seipin. There are other factors also, such as the amount of detergent bound, which was a lower percentage in the purification than for the determination for Stokes' radius [68]. The toroid is a common shape for RNA binding proteins [69], but these are soluble while seipin is an ER protein. Some chaperones also form toroids [70]. This could be another clue to seipin function: Is seipin a membrane protein chaperone? If so, why don't we see binding partners?

Unfortunately, we have not yet improved our yield of seipin sufficient enough to perform detailed structural studies of the toroid macromolecule.

Role of seipin in lipid metabolism

Shortly after we reported yeast seipin, the lab of Hongyuan (Rob) Yang in Australia (Singapore at the time) published a similar screen of lipid droplet morphology in which seipin was also identified [60]. Most of Yang's following papers follow two lines of the story: 1 -seipin is involved in phospholipid synthesis, and this related to the supersized droplets observed in yeast (discussed earlier); 2 -seipin knockdown causes increased oleate incorporation into TAG, and over-expression causes decreased incorporation into TAG in cell lines and mouse models. Both of these indicate that seipin is involved in lipid metabolism.

An interesting, but puzzling finding from the Yang lab is that gene chip analysis, looking for changed expression in the *fld1Δ* yeast strain, revealed that two proteins were significantly upregulated: *INO1* (inositol 3-phosphate synthase, upregulated 5-fold) and *OPI3* (phospholipid methyltransferase, upregulated almost 4-fold). Regarding lipid levels, a modest increase in microsomal PA was present, which has been shown to increase transcription of these genes [71, 72]. The increase in transcription should, theoretically, shunt PA into PI (synthesis of which is controlled by *INO1*) and PC (controlled by *OPI3*). However, while PA is increased over wild-type, there have been no reports of an increase in PI or PC.

Additionally, total phospholipid/TAG ratio is actually decreased compared to wild-type, but this may also be influenced by a modest (25%) increase in TAG (discussed next). So, does *fld1Δ* up-regulate PA formation, which causes the cell to compensate by increasing flux into PI/PC? Or does seipin interfere with the flux of PA into PI/PC, which causes an accumulation of PA and a decrease of overall phospholipid?

I mentioned above that neutral lipid is increased in *fld1Δ* cells, and this is one of the major themes of the Yang lab. The lab reported it first in their LD morphology screen paper as a supplemental figure that showed that *fld1Δ* yeast had twice the whole cell TAG and SE (neutral lipid) as wild type when the cells were grown in rich media [60]. If grown in minimal media, the lab reported later that neutral lipid levels only increase about twenty-five percent [62]. The cause of this increase was not apparent since there was no increase in short-term incorporation of tritiated oleic acid into TAG, although the amount or rate of lipolysis was not mentioned. They also reported mild alterations in the phospholipid-derived fatty acid species as well as the free fatty acid pool. I could not confirm a large increase in TAG or SE in *fld1Δ* yeast compared with wild type. I occasionally noticed a slight increase of TAG in fld1Δ yeast in certain types of media, such as oleate, but the increase was small. In lymphoblastoid cell lines generated from primary lymphocytes of seipin patients, the TAG level was actually reduced [61].

However, analysis of cell lines with altered seipin expression suggested that seipin negatively regulates neutral lipid levels, supporting Yang's results. When seipin is knocked down in HeLa cells or 3T3 fibroblasts (without adipocyte differentiation) followed by culturing in oleic acid-containing medium, both cell types had increased steady-state TAG levels and increased the rate (over two hours) of labeled oleate incorporation into TAG [73]. Conversely, when either isoform of hseipin, tagged with mCherry, is overexpressed in cells cultured in oleic acid, both HeLa and 3T3 cells had decreased lipid droplets, decreased TAG, and decreased incorporation into TAG. Also, a TET promoter (which induces transcription upon docycycline addition) was employed to show that lower seipin expression compared to over-expression decreases droplet formation. Over-expressed [A212P]hSeipin (orthologue to [G225P]ySeipin) was inactive: it did not inhibit droplet formation or change glycerol release (a measure of lipolysis), microsomal TAG formation, or expression of lipogenic genes. In these studies, multiple tags (mCherry, HA, myc) were used to rule out specific effects of a specific tag on lipids or droplets.

In our experience we usually do not see such effects in yeast over-expressing hseipin or yseipin [2]. When I over-express yseipin-mCherry, I have seen a decrease in lipid droplets in a very small fraction of cells that have very intense mCherry signal in certain strains, *4KOfld1Δ* and *4KO* cells (upon Gal-*DGA1* expression) that will be described in Results, but they differ from wild type

in that they are both induced to generate TAG. The HeLa and 3T3 cells in the previously described experiment were also induced to synthesize TAG, so perhaps seipin only affects TAG synthesis when cells are induced to promote TAG storage. Also, the authors always used a tagged version of seipin, which could influence effects on TAG levels. They partially ameliorate this caveat by also expressing a native protein in mice, but they chose to over-express **human** *seipin* (short isoform 2).

In mice, over-expression of hseipin (short isoform) increased basal as well as hormone-stimulated lipolysis in white adipose tissue, measured as glycerol release from cells [74]. The animals also had less total adipose tissue according to MRI, as well as smaller adipocytes and droplets. The decreased lipid in adipocytes is consistent with their findings in cell lines. These mice also had increased mRNA expression of lipases and all perilipins (mammalian LD proteins that help control lipolysis) except Plin2 (ADRP) in white adipose tissue. While only a small increase in non-esterified fatty acids in the bloodstream was shown, the transgenic mice did have increased ectopic neutral lipid storage in the liver. Compared to the over-expression studies, ablation of mseipin (deletion of exon 3 only), lead to a much more severe decrease in adipose tissue amount, droplet size, and resistance to insulin [65]. However, there was no hypertriglyceridemia and only a small increase in cholesterolemia, both of which are severe in human BSCL2 lipodystrophy. The liver displayed ectopic lipid storage with increased mRNA of

fatty acid synthase, Δ9-desaturase (although, as mentioned earlier, desaturated fatty acids were decreased in cells from human patients [61]), and PPARγ in the liver.

Chen *et al*. have also reported the generation of seipin-knockout animals (again deleting exon 3) [64]. As for the results form the Yang lab [65], this group also reported that the animals were lipodystrophic; in addition they found that lipolysis was increased in white adipose tissue (WAT), as was found for transgenic hseipin (short isoform) mice. The animals displayed increased hypertriglyceridemia and plasma NEFA (non-esterified, or "free", fatty acids) after re-feeding and insulin resistance. Importantly, in MEFs (mouse embryonic fibroblasts) differentiated from these mice there was an increase in lipolysis due to an increase in cAMP and PKA (protein kinase A) activity. Basal (unstimulated) glycerol release and basal NEFA concentration were both elevated in *BSCL2*-/- mice WAT. Basal and β3 adrenergic agonist-stimulated glycerol release was higher in adipose explants from *BSCL2*-/- mice compared to those from wild type mice. *UCP1* and other brown adipose-related genes were upregulated at both mRNA and protein levels in *BSCL2* -/- remnant white adipose tissue. Lastly, both aerobic and anaerobic respiration of the mitochondria was elevated in *BSCL2*-/- mice. This indicates that the white adipose tissue uncoupled of lipolysis from ATP production, such that the WAT is behaving like brown adipose tissue (BAT).

As a whole, the *BSCL2*-ablation mice and mice over-expressing short hseipin have the same phenotype of increased lipolysis in their WAT. The data derived from the mice that over-express short hseipin may be artifactual since they are based on over-expression of a human protein in mice. The promoter used to over-express short h*seipin* was aP2, which should limit expression to lipid containing tissues [75]. But what if mice that over-express mouse seipin were to have the same phenotype as mice expressing human seipin? It would indicate that there were two different causes in this mouse model for the same lipolysis phenotype with over-expression of human seipin and ablation of mouse seipin in a mouse model.

Role of seipin in adipogenesis

The most important finding of the Chen ablation mice (BSCL2-/-) is that increased cAMP and lipolysis is the reason for the incomplete adipogenesis in differentiating MEFs. The most well established phenotype for BSCL2 null organisms is the virtual absence of adipose tissue in patients. Thus, many investigations are aimed at showing the involvement of seipin in adipogenesis. Fibroblasts from lipodystrophic patients have decreased levels of PPARγ, lipoprotein lipase, leptin, and GLUT4 [76], indicating that the differentiation program is impaired. Two similar studies looked at BSCL2 expression during adipocyte differentiation, and they found that mRNA increases during

differentiation with hormone cocktail [53, 54]. They also both used short hairpin (sh) RNA to knock down *BSCL2* in 3T3 fibroblasts and C3H10T1/2 mesenchymal stem cells, and this impaired, not early differentiation into preadipocytes, but late stage differentiation. Genes for lipogenesis are decreased, and lipid accumulation is decreased when cells were treated with shRNA. Additionally, Chen *et al.* found that an agonist of PPARγ could rescue adipogenesis, while not increasing expression of *BSCL2* [53]. The rescue of adipogenesis coincided with rescued expression of late genes in the adipogenic pathway: *CEBPα*, *aP2*, and *SREBP1c* (to a smaller extent).

MEFs from seipin-ablation mice had many of the same problems with differentiation as fibroblasts from lipodystrophic patients[64], such as decreased number and size of lipid droplets and decreased *PPARγ*, *C/EBPα*, *aP2*, and *PLIN1* mRNA. However, unlike the previously described studies, adipogenesis was rescued by a lipase inhibitor, not a PPARγ agonist. Experiments were described that were consistent with an important role of lipase stimulation in the *BSCL2*$^{-/-}$ phenotype. Thus, fibroblasts had increased phosphorylation of Plin1 (perilipin) and hormone-sensitive lipase (Hsl) by day 4 (D4) of differentiation. By D4, they also displayed increased total *PLIN2* and *ATGL* expression, and increased cAMP. A PKA inhibitor increased the TAG level in fibroblasts from *BSCL2*$^{-/-}$ mice, and seemed to rescue D12 Plin1 and aP2 protein levels. Increasing cAMP with forskolin or IBMX in wild type fibroblasts decreased cellular TAG and *PPARγ*,

C/EBPα, *GLUT4*, and *PLIN1* expression by D10. Unfortunately they did form Oil red O staining accompanying the change in cAMP. This should show no differentiation due to increased cAMP with the hormone cocktail that normally stimulates adipogenesis.

There are a few potential problems with these ex vivo experiments, the negatively affected differentiation program by D4 caused by rampant lipolysis in *BSCL2*$^{-/-}$ is convincing. However, since lipolysis data were not provided for MEFs without differentiation cocktail, we have to assume there was no phenotype without the induction of adipogenesis. WAT had a steady-state increase in lipolysis, which is good evidence that seipin may actively inhibit lipolysis in WAT. It would have been helpful to know if seipin inhibits lipolysis in other tissues. It is clear that seipin promotes adipogenesis, but it is unclear how that relates to seipin in a non-adipose cell.

C. Lipid droplet Biogenesis

Adipogenesis and lipid droplet biogenesis are closely linked, but there has been no conclusive evidence that seipin has an important role in LD biogenesis. LD biogenesis is a basic, but little understood, phenomenon of cell biology. Interest has grown in this process since it has become clear that LDs are metabolically active and dynamic organelles. There is a controversy over two different models of lipid droplet biogenesis, with both having good arguments.

The most prevalent model is that neutral lipid, know to be synthesized by the enzymes in the ER, start to coalesce in between the bilayer leaflets as a lens-shaped structure, followed by expansion of the neutral lipid depot, which then pulls away from the inner bilayer leaflet, pinching from the outer ER leaflet, and, in some cases, budding from the ER (Figure 4). This is the most accepted model for several reasons. First, lipid droplets are unique organelles in that they have a phospholipid monolayer surrounding neutral lipid, instead of a phospholipid bilayer surrounding a lumen. The phospholipid tails are embedded in, or mixed with, neutral lipid. In order to produce a droplet with a monolayer, forming between a membrane bilayer seems the most energetically favorable process. Second, the biosynthetic enzymes for phospholipid and lipid esters (neutral lipid) reside in the ER, although at least some of them, such as Dgat2 in adipocytes [77] or Dga1p in yeast [78] can be transferred to the LD surface once these droplets are made. Thus, the ER is the most likely site for the birth of droplets. Phospholipid synthesis would be especially critical for this model, since the ER would have to maintain its membrane integrity, yet the phospholipid area would have to increase as neutral lipid bulged out from the surface of the ER. Lastly, this model would allow integral and peripheral proteins to have access to the lipid droplet surface as it was being formed (still connected to the ER), where they presumably concentrate by an unknown mechanism on the nascent LD surface. Isolated lipid droplets have a specific proteome, most likely consisting of proteins that are

resident on the droplet surface. It would be difficult to imagine transmembrane proteins being present in the monolayer with neutral lipids on the trans side. Consistent with the lens model, proteins with targeting domains to lipid droplets are first inserted into the ER, retain the ability to localize at lipid droplets with COPII inhibition (blocking ER to Golgi export), and relocalize to the ER when droplets are catabolically active [79]. The path of membrane protein targeting from ER directly to droplets is an argument for droplets being functionally, and probably physically connected to the ER.

Our lab argues that, at least in yeast, droplets remain connected to the ER [63, 66], and there is also support for this being true in mammals [79]. This would allow the droplets to shrink or grow as the cell requires, with the ER serving as a buffer for phospholipids, and it would also imply that LDs are a specialized subdomain of the ER, like the nuclear membrane. It is well known that droplets can travel long distances directionally and rapidly within the cell in a microtubule-dependent manner in mammalian and fly cells [80]. If droplets were connected to the ER, they would have to either move freely across the surface of the ER (while remaining segregated from it in some way so that LD proteins and phospholipids remain associated with the LD), or droplets would carry a section of ER around with them as they moved on microtubules. There is evidence that LD phospholipid composition is unique from ER [81], so it seems likely that the droplets are segregated from the bulk of the ER. In mammalian cells, some believe the ER-to-

droplet connection was a tubule stalk of bilayer so that transmembrane proteins could be closely associated with the droplet but permit other types of proteins to move freely to the LD surface [82]. This would give more flexibility to the ER-LD connection.

The problems with the budding model are issues with the expansion, budding, and segregation steps of the process. The nascent neutral lipid would have to be restricted to a local area in order to expand the outer phospholipid leaflet in an environment. There is no known mechanism for restriction of neutral lipid to focal points within the ER. On the contrary, there is a huge two-dimensional space of the bilayer in which to diffuse. It has been thought that lipid rafts may serve to "fence in" neutral lipids [83]. Moreover, what prevents expansion in the other direction towards the ER lumen? Is there more resistance to expansion in that space? In sheet-like ER, expansion into the lumen may not negatively affect cells, but in tubular ER, the bulge could occlude the lumen. It is probable that phospholipid generation in the cytosolic leaflet, and not the lumenal leaflet, would encourage the neutral esters to bulge mostly away. This would require local activation of phospholipid biosynthetic enzymes in the ER. The other main problem of this model is the energy required to convert a lens of lipid between the bilayers to a spherical droplet, and then forming the relatively small neck or stalk between the ER and LD, and perhaps completely pinching off the droplet from the ER. This is related to restricting the lipid esters to a local area

that may best be done at an early step before there is a relatively large amount of neutral lipid.

Neutral lipid can exist in the membrane up to a few mol% [84, 85], and if it is above the solubility limit, it is likely to "oil out" in between the bilayer to form a mobile aggregate [86]. This aggregate is more likely to spread in the membrane (more like a lens) than to form a spherical shape [86]. Therefore, there is a need of protein or lipid raft to exclude neutral lipid from the bulk of ER and into a localized lipid droplet. Would transmembrane domains of proteins be enough of a container, or would lipid slip through them like sand through fingers? Protein channels and intramembrane proteases [87] contain hydrophilic pockets in the bilayer, and perhaps this design would be a better lipid fence. The main problem with the model, as stated in reviews [1, 83, 88], is that the lens has never been directly observed, nor any neck or stalk (although LDs are often closely associated with ER membranes and there is evidence for functional interaction [79, 89]), but pores on LDs (that would have continuity with the ER cytosolic leaflet), stalks, and lipid ester lenses might be extremely small and difficult to visualize by normal methods [1].

The main alternative model solves the requirement for a protein-based lipid fence by originating the droplet in a vesicle[90]. This organelle of origin is composed of a limited amount of bilayer, so phospholipid would have to be

synthesized and/or lumen membrane would have to be disassembled gradually to shrink the lumen and allow neutral lipid expansion. The vesicle would transfer to a close apposition to the ER (where phospholipid is made), described as an egg in a cup where transfer of materials has been proposed to occur [91, 92] (Figure 5). It seems unlikely that lipids or non-soluble proteins could diffuse across this space however small it is. If a protein can span three phospholipid layers and have one end be hydrophobic, a protein channel across this space could be envisioned, but the way it could be folded and assembled without the existence of this egg-cup is difficult to imagine, as is the existence of such a channel. However, there is a reason for the egg-cup structure, and it occurs commonly, at least in macrophages [92] and 3T3-L1 adipocytes [93]. The COP machinery, both COPI and COPII is present and one of them could be utilized to synthesize the vesicles proposed to originate the droplets. It is known that COP subunits are required for appearance of some proteins on the LD [94, 95]. Brefeldin A, which inhibits COPI assembly, suppresses lipid droplet formation, albeit incompletely [96], and RNAi of *Drosophila* COPI components affected droplet morphology [97]. It seems more likely, however that COPI machinery are needed indirectly for droplet formation/maintenance for recycling important factors back to the ER from other exocytic compartments. It also seems more likely that, if vesicles were the membrane of origin, that the vesicle would be COPII, which play a role in other transport processes out of the ER, but there is no evidence for this. However, an

attractive element of the egg in cup model is a nascent vesicle/droplet with a lumen sufficient to accommodate biosynthetic transmembrane proteins such as DAG acyltransferase (*DGA1* in yeast) that can contribute to expanding and maintaining the droplet. ER invaginations have been seen inside lipid droplets [98], although this could be due to a droplet on the end of an ER tubule or other artifacts.

I have outlined these models to illustrate how little we know about droplet biogenesis and to illustrate the questions the field faces. We would like to identify genes (encoding elements of the machinery) that are involved in lipid droplet biosynthesis and maintenance. Using yeast genetics, we can benefit by finding phenotypes that can distinguish between models. For example, if we delete the gene(s) involved in sequestering neutral lipid to a microdomain of the ER, we would expect to see flat, lens like droplets or no droplets at all.

The first problem is that droplets may just require neutral lipid to be present to form because the only known way to get a yeast cell with no lipid droplets is to delete all four acyltransferases and no other genes required for droplets have been identified. Droplets appear to only need one of the enzymes that synthesizes neutral lipids, since expression of any one of the four yeast acyltransferases that generate TAG or SE is sufficient to form LD *de novo* [89]. As expected, inhibition of fatty acid synthase with cerulenin results in the net

lipolysis of almost all LD in the cell [99]. Another problem may be redundancy of genes. Lipids can be extremely toxic, especially free fatty acids, and lipid droplets are thought of as a way to sequester and neutralize these toxic biochemicals [100]. Besides redundancy, we feel that there may be a back-up, emergency path to produce ectopic droplets, and, possibly, this is what we see in the *fld1Δ* (yseipin) LD phenotype. Some other problems may be the resolution limit of microscopes and the fact that the most studied droplets are adipocyte or 3T3-L1 droplets rather than droplets that are formed in other eukaryotic cells. Droplets are not all the same: there are differences between the morphology, proteome, and metabolic state of large unilocular droplet in adipocytes and small, multiple, uniform droplets in other mammalian and yeast cells [1].

Besides the caveats and logical lacunae in the lipid droplet biogenesis models themselves, there are other questions about droplet biogenesis. Are droplets initially micro-droplets and then fuse? Are lenses smaller than the limit of detection? Are droplets created and expanded with the same machinery, or are these two distinct steps? Are there scaffolds that coordinate phospholipid and neutral lipid synthesis along with the lipid fence and neck/stalk constriction (and maybe pinching)? What signal defines a LD birthplace? While my data may not convincingly prove an existing assembly model or define a machine in detail, I provide the first evidence that seipin is directly involved in *de novo* lipid droplet biosynthesis.

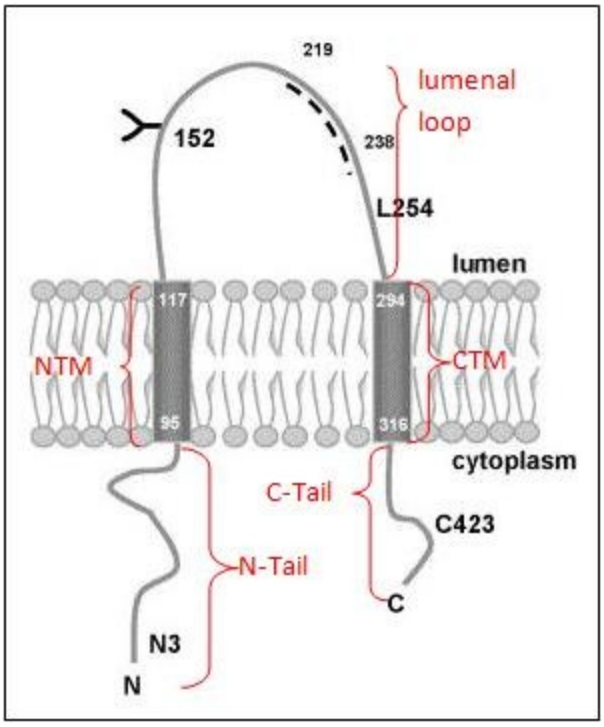

Figure 1. Topology and structural domains of human seipin. The N terminal cytoplasmic tail (N-tail), the N transmembrane domain (NTM), the lumenal loop, the C transmembrane domain, and the C terminal cytoplasmic tail (C-tail) make up the structural domains of all seipins. Shown is the predicted topology of human seipin with the glycosylation motif at asparagine 152 (isoform 1). The lumenal loop is probably more closely associated with the ER membrane than shown. Adapted from **Lundin, C.** ***et al.*** ***FEBS Lett*** **580, 2281-2284 (2006).**

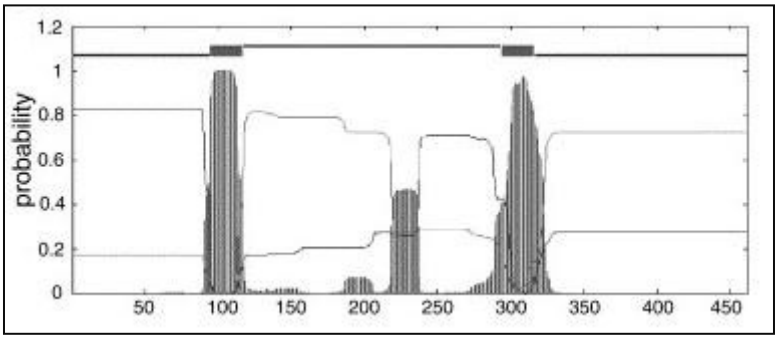

Figure 2. Topology prediction for isoform 1 using the transmembrane hidden Marcov model (TMHMM) prediction method. The Y axis is amino acid number, and the X axis is the probability of being in a transmembrane domain. Notice the weakly predicted transmembrane domain in the lumenal loop domain. Reproduced from **Lundin, C.** ***et al.*****,** ***loc cit.***

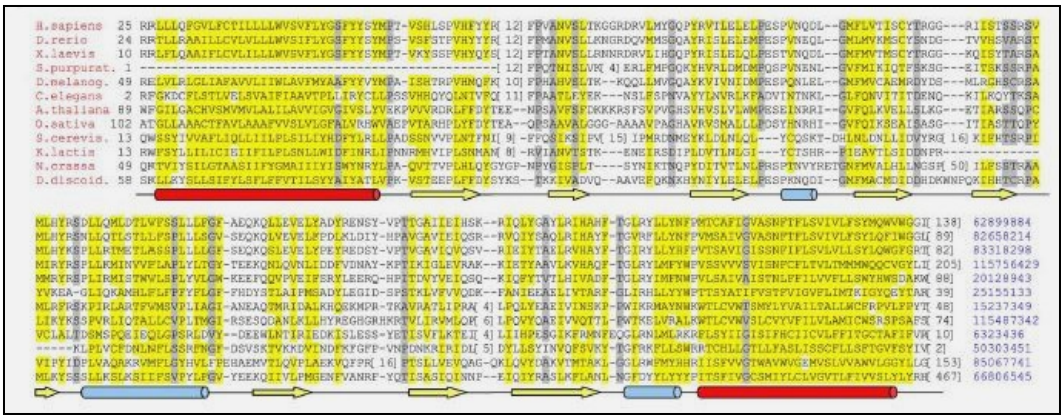

Figure 3. Alignment of several seipins using PROMALS (PROfile multiple alignment with structure). Alignment based on local structure and amino acid type. Notice that most of the homology is in the secondary rather than primary structure. Reproduced from Szymanski, K.M. et al. Proc Natl Acad Sci U S A 104, 20890-20895 (2007).

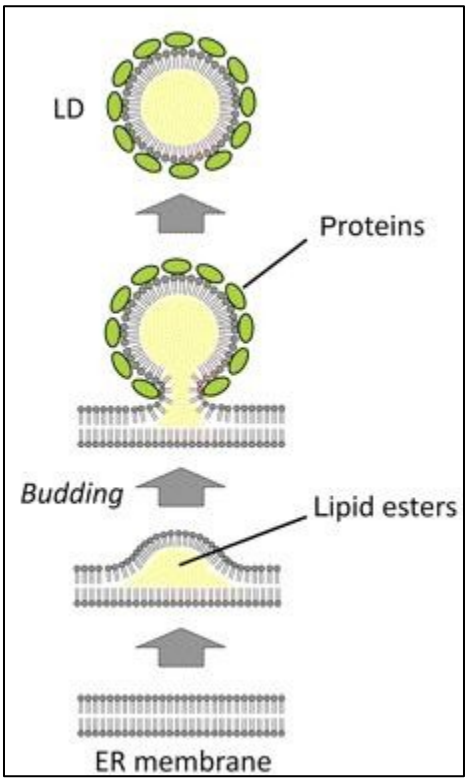

Figure 4. Lens model of LD biogenesis. Neutral lipid esters form between the phospholipid leaflets of the ER, pinch-off, and possibly bud from the ER (although LD probably do not bud off in yeast). Reproduced from **Suzuki, M., Shinohara, Y., Ohsaki, Y. & Fujimoto, T. *Journal of Electron Microscopy* 60, S101-S116 (2011).**[1]

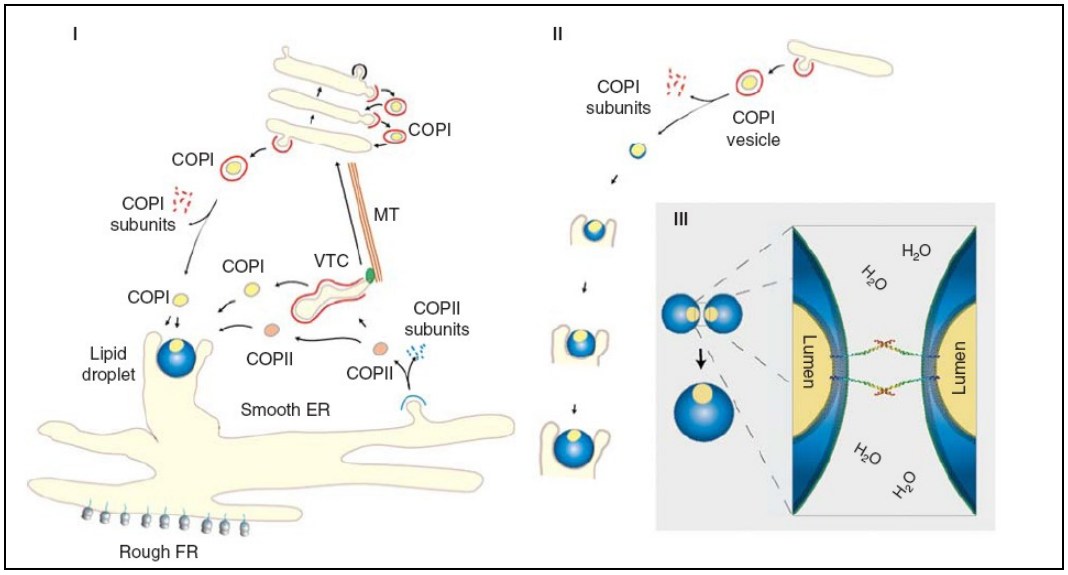

Figure 5. LD Biosynthesis model using COPI coated vesicles to form nascent LD. (I) Normal membrane trafficking of COP-coated vesicles, including to an egg-cup-situated LD being "nurtured" by the ER. (II) Model of LD biogenesis through COPI-coated vesicles. Blue is neutral lipid. Yellow is the vesicle lumen. Reproduced from **Kalantari, F., Bergeron, J.J.M. & Nilsson, T. Molecular Membrane Biology 27, 462-468 (2010).**

Methods and Materials

Induction system and fluorescence microscopy

Yeast cells inoculated from a colony on a plate into 50 ml of glucose synthetic complete growth medium (SCD-yeast nitrogen base (Difco) 6.7 g/L, 2% dextrose, and appropriate base and amino acid supplements: for complete- 40 mg/L adenine, 20 mg/L arginine (HCl), 100 mg/L aspartic acid, 100 mg/L glutamic acid monosodium salt, 20 mg/L histidine, 60 mg/L leucine, 30 mg/L lycine (mono-HCl), 20 mg/L methionine, 50 mg/L phenylalanine, 375 mg/L serine, 200 mg/L threonine, 40 mg/L tryptophan, 30 mg/L tyrosine, 150 mg/L valine, 20 mg/L uracil) and cultured to stationary phase, about 48 hours. All liquid cultures were incubated in a rotary shaker at 30 ^{o}C and 210 rpm. Cells were harvested and diluted to 0.25 OD_{600} / ml into 50 ml raffinose synthetic complete growth medium (SCR-same as glucose, but 2% raffinose instead of dextrose) and grown to stationary phase for 20-24 hours. Finally, cells were washed with sterile water, harvested and diluted to 0.5 OD_{600} / ml into 50 ml galactose synthetic complete growth medium (SCG-same as glucose, but 2% galactose instead of dextrose). Samples (3-5 ml) were removed from the stationary raffinose (SCR) culture and every hour after dilution into SCG medium. Samples were processed by harvesting, re-suspending in 50 mM Tris-HCl, pH 7.5, adding 1 μg (1 μg/ μl stock) BODIPY 493/503 (Invitrogen)/ 500 μl cell suspension, staining 10

minutes, concentrating to about 100 µl, and placing 2 µl on a slide, covered with a coverslip (no sealing), for imaging.

All images for BODIPY were captured with a 100 msec exposure, full field (no artificial magnification), with FITC filter set (Excitation 490/20; Emission 528/38) and a 100X 1.3 NA oil objective in a Zeiss Axioplan 2E microscope equipped with a digital camera (Sensican; Cooke). Three fields of 50-200 cells (typically 150) were imaged per time point. 10 to 20 z-sections were imaged per field with a thickness of 0.3 µm. Images were acquired in Slidebook (version 4.1.0.3; Intelligent Imaging Innovations). The z-sections were deconvolved using the nearest neighbors method, and then a maximum projection (so that the maximum intensity within the stack of each pixel is shown) was made from the deconvolved stacks. Fluorescent body (FB) number was quantified per cell and per field by visual inspection. "Zero" FB cells were not accounted for in the ledger for total FB, but they were accounted for when calculating FB / cell, since the denominator is total cells in a field. Raw FB area was quantified with ImageJ by adjusting a threshold on a 16-bit image of the BODIPY channel to the size of FB and then using the software to calculate an area for each FB (used for Figure 6). The minimum size was set at 1.5 so that every FB 2 pixels^2 and larger were characterized. This was to reduce the number of partial FB getting characterized, since almost all actual FB were larger than 1 pixel 2 (ImageJ only reports whole numbers for the individual FB). Corrected FB area characterized

only the first 25 FB from each quarter of the total tally created by ImageJ. Then I flagged and FB that was 11 pixels^2 or greater, since that was the threshold for a normal-sized FB. Then the outline of FB characterized by ImageJ were compared to the image to make sure each FB was a single FB. If not, that area was divided by the number of partially resolved FB that existed in that FB (as seen by ImageJ), and this number was added to the total tally, which was then divided into the total area of these 100 raw FB for the corrected average FB area (used for Figure 9). The fraction of cells with FBs was calculated from the number of cells with at least 1 FB, divided by the total number of cells in that field. Cells on the edge of the field were characterized only if it was highly likely that more than half of the cell was in the field.

Fluorescence intensity measurements were performed with ImageJ. Images saved at equal minimum and maximum intensity, from three independent experiments, and from 5 hours after switch to galactose medium were used. Twenty fluorescent bodies or cells (for intracellular membrane intensities) were quantified by drawing a line over the center of the fluorescent body or twice over intracellular membranes at two different locations in the cell. Profiles were obtained across the lines (using "Plot Profile" in the "Analyze" menu of ImageJ), and ordered pairs describing the profiles were saved. The peak intensity was calculated by subtracting the highest value from the lowest value of the profile. When quantifying intracellular membranes, I avoided "holes" (areas of the

complete absence of BODIPY signal) created by vacuoles to avoid measuring an artificially low background signal. The holes' borders yielded a sharp steep gradient of signal, so I was able to quantify membranes close to the vacuole without compromising the intensity measurement. Peak width was measured at the inflection at the bottom of the slope. The peak angle was drawn with ImageJ: a vertical line was drawn up from below the peak to the peak, and a second line was drawn connecting the peak with the lowest inflection of the curve, choosing the steeper side of the slope. The software then indicated the angle at the peak between the two drawn lines.

Electron microscopy

Yeast were grown with the induction system described above to 6 hours post-galactose induction and processed according to the Wright protocol as previously described [101]. Briefly, cells were pre-fixed in 0.2 M PIPES, pH 6.8, 0.2 M sorbitol, 2 mM $MgCl_2$, 2 mM $CaCl_2$, and 4% fresh glutaraldehyde over a weekend. Then cells were then post-fixed in 2% potassium permanganate and stained in 1% uranyl acetate. Cells were dehydrated with a graded ethanol series and infiltrated with a graded resin series, ending up in pure resin. Particles of cell were transferred to capsules for embedding and baked in a 60^{o}C oven for 24 hours. Cells were sectioned, re-stained with uranyl acetate, and imaged on an FEI XL30 ESEM microscope.

Lipid analysis

Chloroform/isopropanol extraction − basic protocol. My basic method has been described previously [102], but the protocol was modified during the project. Yeast cells were grown from a plate in 50 ml glucose minimal synthetic growth medium (SD-yeast nitrogen base (Difco), 2% dextrose, and appropriate base and amino acid supplements) overnight, harvested, and diluted in 200 ml SD medium. After 1-2 (average 1.5) doublings, cells were harvested in an ice-cold rotor into pre-weighed ice-cold glass test tubes. Cell pellets were then treated with 2 ml isopropanol at 70 ^{o}C for 30 minutes while covered with foil, and lipids were extracted as described. The chloroform extract was then evaporated under nitrogen at 37 ^{o}C. Dried lipid extracts were usually stored over night at -20 ^{o}C under nitrogen gas.

Dried lipid extracts were dissolved in chloroform (for the basic protocol) or 2:1 chloroform methanol (see below) and spotted on Partisil K6 silica plates (silica gel 60 Å- Whatman) (baked at 260 ^{o}F for 30 minutes and cooled), 5 µl at a time, at an origin 1.5 cm above the bottom of the plate and 1 cm from each other. Plates were developed in a TLC jar equilibrated (for at least 30 minutes) with hexane : diethyl ether : acetic acid at 80 : 20 : 1, filling the tank to 0.5 cm depth, for 50 minutes. For acid charring, plates were sprayed evenly with 3% cupric acetate in 8% phosphoric acid and baked for 10 minutes at 260 ^{o}F about five

times. Lipid spots were scanned in a flat-bed scanner and analyzed using ImageJ. Mass was calculated from a standard curve of lipids (Nu-Chek Prep, TLC 18-5C) spotted on the same plate.

Modifications

Zymolyase- Cells were harvested and treated with Zymolyase 100T at 8 mg/1000 OD_{600} for 45 minutes at 30 ^{o}C. Spheroplasts were weighed and subjected to hot isopropanol, extracted, and analyzed as above.

Glass bead lysis- Yeast pellets were lysed with acid-washed glass beads (Sigma-Aldrich, G8772, 425-600 μm) in lysis buffer (50 mM Tris-Cl pH 8.0, 1 mM EDTA, 150 mM NaCl, 10% (v/v) glycerol, 0.5mM dithiothreitol) containing 0.1% (v/v) IGEPAL CA630 (Sigma-Aldrich I-3021, equivalent to NP-40) in the cold room for 30 minutes. The lysed cells were subjected to hot isopropanol, extracted, and analyzed as above.

Chloroform/Methanol- The chloroform/methanol extraction was a modified version of Bligh and Dyer [103]. Briefly, cell pellets were lysed with glass beads as described above, then the volume was adjusted to 1 ml with lysis buffer. Lysates were treated with 1.25 ml chloroform and 2.5 ml methanol overnight at 4 ^{o}C unless otherwise noted. After extractions were warmed to room temperature in a desiccator, 1.25 ml of chloroform and 1.25 ml of 1 M KCl were added with vortexing prior and after additions. After organic phase was partitioned and

collected, a second washing of the cell debris with 1.9 ml chloroform was performed and collected. Samples were then evaporated under nitrogen and treated as above, except the dried extract was resuspended in 50 µl 2:1 chloroform methanol.

Lipid droplet prep and protein analysis

Highly purified lipid droplets were purified from cells grown to stationary phase in 4 L of SD medium as described by Leber *et al* [104]. The lipid droplets were delipidated as previously described [105] with 2 volumes of diethyl ether. The organic phase was removed, residual diethyl ether was evaporated under nitrogen gas, and proteins were precipitated from the aqueous phase with trichloroacetic acid at a final concentration of 10%. The protein pellet was solubilized in 0.1% sodium dodecyl sulfate (SDS) in 0.1% absolute NaOH (pellets). The protein was quantified by the method of Lowry *et al* [106]. with bovine serum albumin as a standard. SDS-PAGE was performed according to the Laemmli method [107], and the resulting acrylamide gels were silver stained according to Wray *et al* [108].

Glycerol gradients of the seipin homo-oligomer with different detergents [68]

Membranes were prepared based on a published method [109] with several modifications [68]: Spheroplasts were generated with Zymolyase 100T. Before freezing, cells were resuspended at 500 OD600/mL in spheroplast lysis buffer with protease inhibitors. Dounce homogenization was omitted following the 27000*g* centrifugation. When necessary to apply to a glycerol gradient, the

sucrose in the partially purified ER was removed by first adding an equal volume HEPES buffer with protease inhibitors, which was mixed by pipetting, and then centrifuged at 60000 rpm in a Beckman TLA100.3 rotor (RCFav= 152813*g*), 4 °C, 1 h, to pellet the microsomes.

For glycerol gradients, microsomal membranes were dissolved in HEPES buffer with 0.5%TritonX-100 (or other detergent as specified), DTT, and protease inhibitors as described. Instead of 0.5% Triton X-100, we used 0.1% C12E8 (dodecyl octaethylene glycol ether), 2% sodium cholate, 1% CHAPS, and 1% DDM (dodecyl beta-D-maltoside), all mass/volume, as indicated. C12E8, CHAPS, and DDM were obtained from Affymetrix. Cholic acid was obtained from Sigma. Five hundred microliters of the identical buffer containing 15 μL of solubilized membranes and standards was applied to the gradients. The 10 mL gradients containing 10–35% glycerol (v/v) were centrifuged in an SW41 rotor at 35000 rpm 4 °C for 18–19 h. Fractions of 0.5 mL were harvested from the bottom of the gradients, and 19 μL of each was subjected to SDS gel electrophoresis and immunoblotting. The partial specific volumes used for Figure 12 B were previously published [110-113].

ER Stress survival assay

Cells were grown to stationary phase over 48 hours in SD medium, back-diluted into 50 ml of fresh SD medium, and grown about 4 hours for cell OD_{600} to double at least once. Cultures were separated into 5 ml sub-cultures and treated with

indicated amounts of tunicamycin for two hours. Cells were then harvested, and 1250 cells were plated on YPD (rich medium) plates in at least 50 µl sterile H_2O in triplicate, assuming an OD_{600} of 0.1 is equivalent to 3 x 10^6 cells. Plates were incubated at 30 ^oC for 48 hours, images of the plates were taken, and colonies were counted for entire plates.

Results

1. *De novo* biogenesis system

Our hypothesis was that, since *BSCL2* mutations inhibit adipogenesis, *FLD1* deletion will inhibit lipid droplet biogenesis. To test this hypothesis, we needed a method to control LD biogenesis. We had a strain of yeast that is lacking the four acyltransferases in yeast that catalyze the final step in neutral lipid ester formation. These enzymes add the last acyl chain to diacylglycerol to form triacylglyceride (*DGA1* or *LRO1*) or the only acyl chain to sterol to form steryl-ester (*ARE1* or *ARE2*). As stated earlier, yeast lacking these four genes have no lipid droplets, however, expression of one of these four enzymes in this background is sufficient to produce lipid droplets *de novo*. This was known since triple deletion mutants had lipid droplets [114]. Our lab also observed that *FLD1* deletion had no interference with formation of TAG (triacylglycerol) droplets in the *are1Δare2Δfld1Δ* strain or SE (steryl-ester) droplets in the *dga1Δlro1Δfld1Δ* strain (unpublished data), but we knew nothing about the mechanism of biogenesis of these droplets. In the description of experiments presented in this chapter, we term *dga1Δlro1Δare1Δare2Δ* the background strain or "*4KO*", and *dga1Δlro1Δare1Δare2Δfld1Δ*, which we generated, as "*fld1Δ*" or "*4KOfld1Δ*".

We added *DGA1* back to these strains behind a galactose inducible (GAL1-10) promoter on a plasmid (1st generation, previously described by Jacquier *et al*. [89]). The GAL1-10 promoter is fairly tightly repressed by glucose, but induced when the cells are grown on galactose medium without glucose. We also incubated the yeast in raffinose medium between glucose and galactose as a transition derepressing medium to decrease the time between glucose repression and induction. We also expressed GAL1-10-*ARE1* in our plasmid biogenesis system. The expression of *DGA1* (as measured by LD occurrence) was not evident in glucose medium in both log and stationary phases of growth and in raffinose in log phase growth expressed from a plasmid. However, some expression of *DGA1* was evident in some cells reaching stationary phase in raffinose (perhaps due to the age of the colonies on the agar plates from which the liquid cultures were started) in stationary growth in raffinose medium. Nevertheless, we allowed cells to reach stationary phase before switching to galactose medium.

The cell preparation and assay for droplet formation is fairly straightforward and described in detail in Methods. Briefly, cells from plates were inoculated into glucose complete synthetic medium and grown to stationary phase (generally 2 days), then transferred to raffinose medium and again grown to stationary phase. Finally, a sample for "time 0" was taken from the stationary raffinose culture, and then transferred to galactose medium. At indicated times

after transfer of cells into galactose medium, samples were removed from the culture for imaging. They were washed with a Tris buffer to remove galactose, and then stained with BODIPY 493/503, a dye with high affinity for neutral lipid, for ten minutes. Lastly the cells were concentrated by centrifugation and imaged by epifluorescence microscopy.

As mentioned above, there were a few cells with droplets at time 0 (typically 3-8%), and both the numbers of such cells and average droplet number per cell are fairly constant until three hours after transfer to galactose medium, at which time new droplets start to form (Figure 6 A and B). These two parameters continue to increase until seven hours after induction, when droplet formation starts to plateau. If samples were taken twenty-four hours after switch to galactose medium, the numbers were barely higher, although droplets were larger and stained more intensely (data not shown). This probably indicates that droplet formation is mostly completed by seven hours after induction, but organelle expansion is possible after this time.

It is important to note that the GAL1-10 promoter heavily overexpresses the open reading frame that it is driving, even compared to the *PGK* promoter we also use in the lab to overexpress proteins. Therefore, the induction system is artificial in that unphysiological levels of Dga1p are produced at some point, and this drives droplet formation. It is possible that more time would be required to

form lipid droplets if *DGA1* expression were from its natural promoter. It is also possible that normal cellular capacity of droplets is surpassed in our system, let alone affected by environmental conditions and cell cycle. Despite these caveats, we can still compare the *4KO* to *4KOfld1Δ* strains to determine whether *fld1Δ* affects lipid droplet biogenesis. Also, while LD biogenesis may be accelerated in our system compared to wild type, the same mechanisms are likely employed to create a droplet in a triple deletion mutant (i.e., lor1Δare1Δare2Δ) as in our *4KO* expressing *DGA1*, especially at early time points. Another caveat is that droplets made only of TAG (or SE) may not use the same machinery for assembly, but the added strength of our system is the ability to dissect *fld1Δ* effects on TAG versus SE packaging by exchanging GAL-*ARE1* for GAL-*DGA1*.

Our lab and that of Yang, characterized droplets in *fld1Δ* cells (in the wild type background) as either clusters of small droplets or larger than wild type, supersized, droplets [2, 60]. The difference between a supersized droplet and a cluster of small droplets, however, is often not easy to discriminate by fluorescence microscopy. For this reason, I use the term "fluorescent bodies" (FBs) to describe generally round spot of BODIPY signal which exceeds background by eye (sometimes difficult to differentiate, in *4KOfld1Δ*). Since a cluster of droplets, as seen by electron microscopy, may appear as a single fluorescence spot, I use "fluorescent bodies" (or FB) when interpreting

fluorescence data. However, a single fluorescent body may represent a single lipid droplet in *4KO* and some *4KOfld1Δ* cells. Therefore, a spot was counted as multiple fluorescent bodies if I had reason to believe it represented multiple lipid droplets (i.e. a peanut shape is counted as two, or a three-lobed clover shape as three). Moreover, if there was a visible decrease in intensity between two irregular FBs, indicating partial resolution, they were counted as two. Yeast with the *FLD1* deletion often had very irregular fluorescent bodies (FBs), for example, a fuzzy or irregular perimeter, or weaker fluorescence intensity than wild type, but I kept the same standards for all strains.

A. Seipin deletion inhibits the dynamics of TAG droplet formation

When I first imaged the *4KO* and *4KOfld1Δ* strains during galactose induction of Dga1p, later time points had obvious differences between the two strains, but differences in the early time points were not obvious by superficial visual inspection (Figure 6 A). Therefore, I quantified FB numbers (Figure 6 B, left panel) and size (Figure 6 C, left panel) in the two strains during induction. I found in the *4KOfld1Δ* strain a large decrease in average numbers of fluorescent bodies per cell at all time points from 3 hours after switch to galactose and small, but nevertheless statistically significant parallel decrease in the fraction of cells

with FBs in the same time frame. There was also a large an increase in the average size of fluorescent bodies (discussed more below) from 4 hours on.

There appeared to be no delay in droplet formation the *4KOfld1Δ* strain, since both strains start to produce droplets at the same time (3 hours after switch to galactose, T3). Although not apparent on the graph (Figure 2 B, left), the average FB number per cell increases 3-fold between T2 and T3 (0.259 at T3) and again 3-fold between T3 and T4 (0.905 at T4). This is similar to the control (*4KO*) strain in which a 3-fold increase was seen between T2 and T3 and a 2-fold increase between T3 and T4. Neither strain increased droplets between 0 and 2 hours. I conclude that *4KOfld1Δ* yeast began droplet formation at T3, at the same time as *4KO* yeast. Additionally, GAL-induced Dga1p-myc is detected in a western blot at T4, but not T2.5 in both *4KO* and *4KOfld1Δ* cells, indicating that Dga1p-myc expression occurred in the same time frame as the initiation of FB production in *4KO* and *4KOfld1Δ* cells (Derk Binns, unpublished data). Finally, new FB production in both strains began to plateau at 7 hours, as measured by FB/cell, fraction of cells with FB, and average FB area (Figure 6 B and C). In more recent studies in the lab in which the *GAL*promoter-*DGA1* fusion was placed in the chromosome (at the DGA1 locus) instead of expressed on a plasmid, a 2-hr delay in FB production in the absence of *FLD1* was clear. It is reasonable that the difference in the two expression systems reflects a fraction of cells with plasmid-driven expression produces more enzyme from a larger plasmid copy

number, and this may buffer the difference in formation dynamics of FB between *4KO* and *4KOfld1Δ*. With more homogenous, synchronized induction of Dga1p expression from the chromosome, latent differences in FB dynamics may be uncovered.

In my system, while the kinetics of FB formation (i.e., the time at which droplet numbers increase and plateau) was similar for both strains, there were clearly fewer FBs per cell, statistically significant at all time points starting at 3 hours after switch to galactose medium (Figure 6 B, left panel). This was even reflected at early time points, although there was no significant difference between the low numbers of FBs at earlier time points. FBs in *4KO* yeast started at an average of 0.2 per cell, reach about 6 per cell by T7 when droplet formation plateaued, and slowly climbed to 7 per cell by the end of my measurements (Figure 6 B, *4KO*, left panel). In contrast, *4KOfld1Δ* yeast started at an average of 0.1 per cell, reached about 2.4 per cell by T7, and only increased to 2.6 per cell by the end of the experiment (Figure 6 B, *4KOfld1Δ*, left panel). Therefore, there is a lower starting point and a much lower plateau point of the curve in the *4KOfld1Δ* strain compared to the control.

As mentioned above, there was an apparent lower rate of FB production in *4KOfld1Δ* cells compared to *4KO* cells (Figure 6 B, left panel). Between 3 hours

and 7 hours, *4KO* yeast developed fluorescent bodies at a rate of 1.26 FB/cell/hour, compared to *4KOfld1Δ* yeast with a rate of 0.54 FB/cell/hour; these rates are extremely significantly different from each other. But this does not necessarily imply fewer droplets (as opposed to FB) in the *4KOfld1Δ* strain, which contained clusters of droplets that could not be easily resolved by fluorescence microscopy. We cannot conclude that less TAG was being packaged into droplets or that droplets were produced at a slower rate in *4KOfld1Δ* yeast. Therefore, we cannot conclude from these data that seipin is facilitating droplet formation, by acting as a valve, lipid channel, or another mechanism. Another interpretation of the data presented in Figure 6 A and B is that the *4KOfld1Δ* droplets were fusing or clustering at a rate high enough to counter LD production so that the rate of FB formation appeared low. The droplets could also be in a futile lipolysis/biogenesis cycle, where lipolysis is higher in *4KOfld1Δ* compared to *4KO* yeast, resulting in fewer droplets. Another difference could be the population of cells producing droplets could be lower in *4KOfld1Δ* yeast or *4KOfld1Δ* yeast are not as healthy, although this is probably not the case since the rate cell doubling, a good measure of yeast cell "health", is similar in both strains. Cell morphology, as visualized by bright field optics under a 100X objective, suggests that both strains reacted similarly to culture at all time points. There was no obvious difference in the morphological attributes between the two strains.

Cells of both strains had multiple vacuoles or a single large one, and only a small number of cells displayed a granular cytosolic appearance or an irregular shape that would suggest "ill health." Only about 1% of cells from either strain appeared lysed or dead. (Similarly there was no difference in the number of cells stained with the vital dye Sytox Green between wild type and *fld1Δ* (Bethany Cartwright, unpublished data)). There was no evidence that the *4KO* background sensitizes yeast to the *FLD1* deletion, but it is difficult to rule out the possibility that the *4KOfld1Δ* yeast have subtle general deficiencies compared to the *4KO* control.

To determine whether the difference in the rate of FB formation between the two strains was caused by a higher fraction of cells with no droplets in the *4KOfld1Δ* strain, we determined this parameter. The number of cells with droplets during the time course was similar in both strains, although the number of *4KO* cells with droplets was slightly, but significantly higher than in the *4KOfld1Δ* cells at most time points (Fig. 6B, right). Once formation starts to slow at the later time points, differences were more obvious. The *4KOfld1Δ* mutant plateaued at 55% with droplets, while *4KO* plateaued at 70% (Figure 1 B, right panel). The slopes from T3 to T7, however, were not significantly different (0.121 for *4KO* and 0.107 for *4KOfld1Δ*). One possible interpretation to explain the difference is less tolerance for, or less expression of, plasmids in general in the *4KOfld1Δ* strain. It could also indicate that *4KOfld1Δ* cells are having more

difficulty forming droplets, leading to the lower fraction of cells with any droplets.

By inspection, the fluorescent bodies in *4KOfld1Δ* appeared to be not only fewer in number, but also much more heterogenous in size, and resulted in a larger average area in projection images (Figure 6 C, left panel). The average area was only 14% higher at T0 in *4KOfld1Δ* yeast, and this small difference disappeared in T1-T2. The decrease in average FB size from T0 to T3 was most obvious between T0 and T1. At T3, the average area of FB in *4KOfld1Δ* started to be larger than FB in *4KO* by 25%, and the difference became significant from T4 to T9. At T4 and T9, the difference in average size was 53% and 86% higher in *4KOfld1Δ* cells, respectively. Between T3 to T9 the average area grew at the rate of 1.82 pixels^2/ hour in *4KO* cells and 4.32 pixels^2/ hour in *4KOfld1Δ* cells, resulting in over a 2.4-fold increase in area. This could represent the fusion or aggregation of nascent droplets in the *4KOfld1Δ* strain. Electron microscopy suggested that the large FB represent clusters of tiny droplets (see below); we saw no morphological evidence of fusion at early time points of LD biogenesis, although fusion likely occurs later in *4KOfld1Δ* cells, as suggested in earlier reports [2, 60].

The cause of the decrease of average size between T0 and T3 is unknown, but there were probably two contributing factors. First, lipid droplets become subjected to high rates of lipolysis when stationary cultures are diluted into fresh medium; we have observed this (unpublished) as have others [63]. This occurs probably because lipid from droplets is needed for membrane formation during cell division for daughter cells. In stationary phase lipid can be stored as a bulwark against starvation or for anticipation of future rounds of division. A second potential cause for the decrease in volume of droplets in the early hours of galactose induction of Dga1p is that the FB that were scored do not actually represent droplets. Some of these were very dim and large, and some of these appeared to have a higher intensity rim around the outside as if they were labeling large vesicles. I did not score ones that were obviously vesicles, but I scored the other ones because they were in both strains, although at a slightly higher frequency in *4KOfld1Δ* yeast. These dim FBs at early time points may be neutral lipid-pregnant membranes that when viewed at a certain angle appear to form a spot.

To compare the heterogeneity of FBs in the two strains, I measured FB area at a single time point, 5 hr after switch to galactose medium (Figure 6 C, right panel). I measured 255 FB in *4KO* and 322 FB in *4KOfld1Δ* cells. The peak of distribution of the average size of FB in *4KO* cells was much narrower than in *4KOfld1Δ* cells, which was more broad and flat, as expected from visual

inspection. The range of areas was 2-24 pixels^2 for FB in *4KO* cells, compared with 2-82 pixels^2 for FB in *4KOfld1Δ* cells. The median was almost two-fold higher in *4KOfld1Δ* cells: 13 compared to 7 pixels^2 for *4KO*. This raises an important question. Are these FB in various stated of aggregation, or are the aggregates in various stages of fusion? In other words, are *4KOfld1Δ* droplets generated simultaneously (like an explosion) from a site on the membrane, or do they aggregate from different sites to a location in which they will fuse.

In summary, seipin deletion affects lipid droplet biosynthesis of TAG-filled lipid droplets. Fluorescent bodies were fewer in number per cell and larger in FB area in *4KOfld1Δ* yeast during biogenesis, and seipin deletion causes a broader distribution of FB areas in yeast.

B. TAG is packaged less efficiently into droplets in *4KOfld1Δ* cells

After finding that fluorescent bodies are fewer but larger without seipin in the *4KO* background, we then asked whether levels of TAG are the same. Is the defect in biogenesis due to TAG packaging, or is the defect in TAG formation by *DGA1*? We used the same basic culturing procedure for galactose induction, but with larger cultures to allow 500 OD_{600} units of cells for each time point. We used glass bead lysis to disrupt the cell wall, and then we extracted lipids in chloroform: methanol overnight. *4KOfld1Δ* yeast initially started with less TAG,

but by the end of the assay at T5, the TAG levels have almost reached the levels of *4KO* yeast (Figure 7 A, left panel). The slopes were not significantly different from T3 to T5. I was interested in what the curves would be if the yeast had the same amount of TAG at the beginning of the galactose incubation. In experiments performed subsequently by Derk Binns in the lab with the chromosomally expressed GAL-driven DGA1, TAG levels were virtually undetectable before the galactose switch and were very similar throughout DGA1 induction although there was a large delay in droplet formation without seipin (Hilton, Binns and Goodman, manuscript in preparation). Together, these data indicate that seipin affects packaging *per se*.

C. Fluorescent bodies in the absence of seipin have more indistinct borders and are dimmer, consistent with droplet aggregates.

Seipin deficient cells had fewer fluorescent bodies, but they had equal TAG levels. Where was the TAG if it was not in droplets? Some of the volume was compensated by the larger fluorescent bodies that *4KOfld1Δ* (and *fld1Δ*) cells produced. If a spherical volume was calculated from the average area of fluorescent bodies measured in Figure 6, mathematically converted into an average spherical volume of a fluorescent body, and then the average spherical volume was multiplied by the average number of FB per cell, the volume of droplets per cell between the two strains was equivalent throughout the time

course (Figure 7 A, right panel). This suggested that the amount of TAG in droplets was equivalent, but it assumed equal densities of TAG within fluorescent bodies in the two strains, and a spherical shape of the FBs. I first thought that *4KOfld1Δ* cells did not have spherical FBs because more of them had irregular, non-circular shapes, but also they appeared "ghost-like" - dimmer with less defined borders (Figure 6 A, especially T0 and T4). I used line scans across fluorescent bodies in maximum projection images from serial image stacks of *4KO* and *4KOfld1Δ* yeast saved at equal minimum and maximum intensity values. A line scan will measure the intensity of a channel where the line is drawn, and the FBs will appear as a peak (as illustrated in Figure 7B, left panel). I could not use this technique to demonstrate less solid fluorescent bodies, but dimmer FBs should be apparent by a lower maximum intensity. Also the angle between vertical at the highest point of the peak and the base of the peak should be greater if the border of the FB is more diffuse or fuzzy (illustrated in Figure 7 B, left panel, quantified in Figure 7 C-ii). If the border is sharp, the sides of the peak will be steep. If the border is diffuse or fuzzy, the slope will be more gradual. That is indeed what I found in *4KOfld1Δ* compared to *4KO* FBs. There was a 32.3% decrease in peak height (Figure 7 C-i), a 41.4% increase in peak width (Figure 7 C-iii), and a two-fold increase in the angle between vertical and the peak base (Figure 7 C-ii). The averages of many peaks aligned by the maximum value were graphed in the right panel of Figure 7 B, and it is clear that all three attributes

were different in the two strains. This suggests that many *4KOfld1Δ* fluorescent bodies are not single lipid droplets but aggregates; the cytoplasm between the droplets in the aggregates would make them appear dimmer with less distinct edges.

D. TAG may remain in membranes in *4KOfld1Δ* cells

If we cannot assume the *4KOfld1Δ* fluorescent bodies represented solid lipid droplets, perhaps a fraction of TAG has not been packaged into droplets and was trapped in membranes. We previously showed that BODIPY very lightly stained cell membranes allowing their visualization by the dye at a high "gain" setting with the microscope software [66]. If *4KOfld1Δ* membranes have excess TAG in them, the intensity of BODIPY staining should be higher. Again I employed line scans, and I tried to cross ER membranes two times with the same line since they seemed to be different intensities throughout the cell. The background seemed to differ throughout the cell too. Therefore, I took the highest intensity reached in the line scan and subtracted the lowest intensity from the line scan for background. In drawing the lines, I avoided regions of cytoplasm (presumably vacuoles) when taking measurements. The intensity of staining of membranes in *4KOfld1Δ* at T1 was 10% higher than in the *4KO* strain, but the difference was not statistically significant. However, at T3 and T5 the difference increased to 29% (at both time points) and this was highly significant (Figure 7

D). This strongly suggests that there was more TAG in the membranes in *4KOfld1Δ* yeast compared to *4KO* yeast. The laboratory is presently comparing TAG in isolated membranes from the strains to see if my observation can be confirmed biochemically.

E. Seipin deletion negatively affects LD size and positively affects FB size

The diffuse morphology and lower BODIPY-stained density of a large fraction of fluorescent bodies in *4KOfld1Δ* suggests that they represent clusters of small droplets. To confirm this, I next prepared samples for electron microscopy using permanganate staining to enhance membrane contrast [101]. Cells were harvested 6 hr after galactose addition. Duplicate samples were processed and analyzed for *4KO* and *4KOfld1Δ* cells. Almost no supersized lipid droplets were seen. There were some large, electron sparse, circular structures in *4KOfld1Δ* cells that are often associated with, and in, what are probably large vacuoles (very electron-dense structures- Figure 8 H), but they are also present in the *4KO* cells (Figure 8 G). They were equally large in both strains, and some had inclusions of medium electron density (grey particles). Several of them could represent tears from sectioning, and they were equally present in both strains. Since both strains showed these patterns at similar frequency and did not correspond to droplets seen by fluorescence, I conclude that these structures are probably not lipid droplets,

and supersized droplets are rare in our biogenesis system, at least up to 6 hours after switch to galactose medium.

In contrast, many of the clusters of small electron-sparse structures (presumably LDs) were seen in *4KOfld1Δ* cells, and they were 3-fold more abundant than the *4KO* control (Figure 8 A-D and panel E). A cluster was defined as 3 LDs in close proximity (~200 nm), so the definition was not very stringent. However, there was a large difference between a *4KO* cluster and a *4KOfld1Δ* cluster in that the density of droplets within the cluster (comparing the number of droplets within the cluster compared with the overall area of the cluster) in the *4KOfld1Δ* strain was 8-fold higher than *4KO* clusters (Figure 8 F). These data from ultrastructure strongly suggest that the large diffuse fluorescent bodies that characterize the *4KOfld1Δ* strain represent abundant clusters of small lipid droplets. Seipin, therefore, appears to prevent the formation of normal sized droplets, although I can't rule out that seipin prevents the fusion of tiny droplets into larger ones. However, since dense clusters of tiny droplets are virtually absent in the *4KO* strain, I favor the hypothesis that seipin in to prevent the formation of the clusters of tiny droplets. My data are consistent with droplet morphology at steady state in *fld1Δ* cells, characterized by dense clusters of droplets enwrapped in ER[2, 60]. Morphologically chaotic, tiny droplets were also seen in cells derived from BSCL2 patients [2, 61].

F. Seipin deletion may cause ectopic formation of LD in nuclei

Besides frequent clusters of small droplets, I also observed by electron microscopy of *4KOfld1Δ* cells droplets in the nucleoplasm, usually close to the membrane envelope. Intra-nuclear droplets within cells were found 40-times more frequently in *4KOfld1Δ* than in the *4KO* strain (Figure 8 J). Only 1 in 132 *4KO* cell sections that had a nucleus had this phenotype, while 27 out of 125 *4KOfld1Δ* sections with a nucleus showed this phenotype. While I view this difference as meaningful, the result was not statistically significant because the percentage of nuclear droplets in the *4KOfld1Δ* cells differed in the two duplicate samples: 17% and 32%, compared to 0% and 1.14% for the *4KO* strain. Nevertheless, intranuclear droplets were virtually absent in *4KO* and easily observable in the *4KOfld1Δ*.

In a manuscript in preparation, our lab will propose that seipin is a valve that releases neutral lipid into "proper" LDs, and that seipin deletion leads to increased membrane TAG resulting in bilayer instability, which causes unregulated ectopic blistering of lipid droplets. If this is the case, droplets in *fld1Δ* yeast should be abnormal and possibly dysfunctional in some way without the seipin-mediated regulation of assembly. There is no evidence with starvation assays that *fld1Δ* yeast are less "fit" (Cartwright, unpublished observations).

There are some data that I will discuss later that indicate that LD in *fld1Δ* yeast have a modified protein composition compared to WT cells, and it is already known that LDs in *fld1Δ* yeast are fusogenic and heterogenous in size [2, 60]. My data from the EM, however, supports our hypothesis, since LDs from *4KOfld1Δ* cells originate from abnormal locations such as the outer leaflet of the inner nuclear membrane. We cannot rule out the ectopic droplets we observed were due to improper localization of Dga1p in the absence of seipin. Ectopic droplets may also have been artifacts of processing the samples for electron microscopy, although if so they were specific for *4KOfld1Δ*. I would argue that if there was a sectioning artifact and LDs did not bud into the nuclear matrix of living *4KOfld1Δ* cells, they were at least associated with perinuclear ER more often in *4KOfld1Δ* cells compared to *4KO* cells, where they appeared to be more dispersed.

G. Seipin TAG clusters are not wrapped by membranes when they are born

Our laboratory had previously shown that lipid droplet clusters in *fld1Δ* cells in the wild type background (at steady state) are often enwrapped in ER membranes, resembling "tangles" [2]. The final interesting observation from my electron microscopy images, was that TAG LD clusters in *4KOfld1Δ* cells did not

have membranes wrapped around them, at least not at T6 (Figure 8 D and Figure 14). Therefore, either SE (missing in our *4KO*-derived strains) induces the membrane wrapping that we see in *fld1Δ* yeast, or, more likely, the membrane tangles are a cellular compensation/adaptation mechanism. However, even at T6, the small droplets in a cluster were often associated with membrane fragments we assume to be of ER origin that were rarely observed in *4KO* cells (Figure 14, arrows). The appearance was often of beads of tiny lipid droplets emanating from a localized region of the membrane, suggesting chaotic budding clearer here than we had previously observed in *fld1Δ* cells continuously grown. It remains to be seen if a similar scenario emerges from cells expressing GAL-*ARE1* in the *4KO* background to rule out a specific effect of TAG itself. Also, it will be useful in the future to include wild type and *fld1Δ* controls, grown under parallel culture conditions to rule out effects of our raffinose-galactose protocol. These controls should also be performed to understand the lack of supersized droplets (observed normally in *fld1Δ* cells in minimal medium toward stationary phase) in our experiments.

H. Seipin promotes SE droplet formation, but to a lesser extent than in TAG droplet formation

To determine whether seipin is involved specifically with packaging TAG compared to SE, I repeated the galactose-induction experiment in *4KO* and *4KOfld1Δ* strains but with the GAL promoter driving expression of the steryl acyltransferase Are1p. Compared with GAL-*DGA1*, I had a much harder time distinguishing differences between the two strains expressing GAL-*ARE1* by visual inspection (Figure 9 A). However, quantifying fluorescent bodies (from one experiment with three fields each time point) revealed a modest difference in the two strains (Figure 9 B and C). The results from Gal-*ARE1* expression showed fewer fluorescent bodies in the *4KOfld1Δ*, a significant decrease at most time points, and an increase in the size of fluorescent bodies at later time points. The experiment was repeated two more times, and the images looked extremely similar upon visual inspection, but they were not quantified.

There was a significant decrease in the average number of fluorescent bodies per cell from T3 to T9 (except T4 and T8: Figure 9 B, left panel) in *4KOfld1Δ* cells compared to *4KO* cells, as we saw during Dga1p induction. Like Dga1p expression, *4KOfld1Δ* initially display a two-fold increase in average FB per cell (0.12 compared to 0.21), and this decrease in *4KOfld1Δ* cells compared to *4KO* cells continues from T2 to the end of the time course (the averages are equal at T1). The slopes of linear regressions, taken from T2 to T6, also differ

significantly between the two strains (1.13 FB/cell/hour in *4KO* and 0.89 FB/cell/hour in *4KOfld1Δ* cells), as expected. An interesting result is that steryl-ester FB appear slightly earlier than triacylglycerol FBs, between T2 and T3 for SE (Figure 9 B, left panel) compared to between T3 and T4 for TAG (Figure 1 B, left panel). This may imply that droplets composed of steryl-ester budded easier, or faster, or that the time of protein production is shorter for *ARE1* than *DGA1*, but experiments were not performed to test this idea.

The difference between FB size in the two strains was much smaller for SE fluorescent bodies in the *4KO* and *4KOfld1Δ* yeast, and the differences were only significant from T7 to T9 (Figure 9 C). However differences for other time points may become statistically significant with quantification of repeats of this experiment. Similar to GAL-*DGA1* expression, there may be growth and lipolysis of FBs in cells expressing GAL-*ARE1* from T0 to T3, since the size of FB in both strains seemed to rise and fall during this part of the time-course. However, with GAL-*DGA1* expression the size only decreased during this time (Figure 6 C). An important note about quantifying the area during 0 to 2 hours after switch to galactose medium is that there were so few droplets, that a really large FB (or a few small FB) can alter the average significantly. Therefore, quantifying multiple experiments is important at these early time points. There were enough FBs to have more confidence in the data at T3 and later time points, when difference in sizes of FBs between the two strains was clearer, reaching statistical significance

at T7, as *4KO* droplets become smaller and those in *4KOfld1Δ* become larger: A positive slope (0.17 pixels^2 / hour) for *4KOfld1Δ* and a negative slope (-0.24 pixels^2 /hour) for *4KO*. It would be interesting to see if some of the differences for earlier time-points became significant with more trials, and if the slope of the change in area during GAL-*ARE1* induction in *4KO* yeast actually approaches zero or if it remains negative (*i.e.*, shrink of droplets).

Overall, results from these data demonstrated that seipin deletion droplet size and number for both TAG and SE fluorescent bodies, but the differences were more modest for the latter. The best example of this was average FB size, since the differences did not become significant until T7 when *ARE1* is assumed to be highly over-expressed, and the size of *4KOfld1Δ* SE FB does not reach that of that of TAG FBs in experiments described previously. The slopes of linear regression of the data from T3 until the end were significantly different, so seipin deletion still affected the rate of FB growth in size. I would be unable to conclude that *4KO* and *4KOfld1Δ* FBs are equal in structure (*4KOfld1Δ* FBs could still be clusters, just smaller) without electron microscopy. Another interesting result from the average size curve was that it does not reach a plateau; it is possible that the area of *4KOfld1Δ* FB may reach that of TAG FB if the experiment continued for several more hours.

The differences in FB number with *ARE1* expression echoed the *DGA1* data closer than average FB size, but again the differences were smaller. The fraction of cells with SE droplets was very similar to the fraction of cells with TAG droplets. However, there did not seem to be a lag with SE droplet production. A shorter lag was reiterated in FB/Cell, but not in average size, where the beginning of the linear section of the curve started at T3. If you assume that seipin deletion causes ectopic droplet formation, do ectopic droplets made of steryl-ester blister from the membrane more easily than ectopic droplets made of triacylglycerol? Since cholesterol can increase the stiffness of membranes, and sterol might be in excess when TAG LD are made (since there is no steryl acyltransferase in these cells) but not when SE LD are made, steryl-ester droplets may bud more readily than TAG droplets. If we could use cyclodextran to remove the excess sterol from *4KOfld1Δ* yeast expressing GAL-*DGA1*, an increased rate of droplet formation would be consistent with this idea. Another explanation for a smaller effect of seipin on SE droplet formation compared to formation of TAG droplets is that seipin functions in TAG packaging but there is an unknown, partially redundant activity for SE packaging. Finally, if seipin is involved in inhibiting lipolysis, it is possible that the enzyme that it regulates has more activity towards TAG than SE.

In summary, seipin deletion affects lipid droplet biosynthesis of SE-filed lipid droplets, but to less of an extent than TAG LD. Fluorescent bodies were

fewer in number per cell and larger in FB area in 4KOfld1Δ yeast during biogenesis. More experiments expressing GAL-*ARE1* need to be quantified to have full confidence in the data.

2. Problems with Protocols: Lipid Analysis

Fei *et al*. in 2008 reported differences in neutral lipids between wild type and *fld1Δ* yeast [60]. Specifically, they found a two-fold increase in TAG and SE in log-phase cells growing in rich (YPD) medium, and they stated that this increase also was found in stationary phase or in minimal medium in both growth phases. They also reported no difference in radioactive oleate incorporation into TAG, but a 70% increase of incorporation into SE, compared to wild type cells.

I spent years trying to confirm the steady-state data to begin to study the mechanism behind the differences. I started by using a lipid extraction protocol from used in plants by a collaborator in past efforts of the lab, Dr. Kent Chapman at U. North Texas. The protocol involved initial extraction of a cell pellet in hot isopropanol without a cell disruption step such as vortexing with glass beads or digestion of the cell wall with enzymes. Since this was not necessary for the complete extraction of lipids in plant tissues, we assumed this would be true for yeast as well. Most published yeast protocols for lipid extraction involved cell lysis with homogenizers, but since we did not have this equipment in the lab, we

were hoping to avoid this step. We also started normalizing our loading of lipid extracts on TLC plates based on cell wet weight. Fei *et al*. , after densitometry of lipid spots on TLC plates, seemed to normalize results based on protein in extracts, although this is not made clear in the paper [60]. In SD (minimal) medium, we initially found a 70% increase in TAG with no increase in SE in *fld1Δ* cells (wild type background) (8.9 *vs.* 14.9 nmole lipid / ug protein, Figure 10 A). These differences in TAG levels varied between these experiments to the extent that the difference was not significant. Results from Fei *et al*. in a subsequent paper on supersized droplets showed that the increase in neutral lipid was only about 25% in minimal media [62], indicating some inconsistency in their lab as well.

During my studies on lipid composition in *fld1Δ* cells, I noticed that there was an increase in free (non-esterified) fatty acids (FFA) when cells were cultured in SD minimal medium, and I found this was true for the *fld1Δ* deletion in two wild type strain backgrounds: an 80% increase of FFA in the BY4742 strain (Figure 10 A), and 60% in the MMY011α strain (data not shown). For several months these differences were reproducible, and so I turned my focus to try to understand the basis for the FFA increase in *fld1Δ*. I manipulated the expression of several genes (including generating gene knockout) to try to understand the basis for the *fld1Δ* phenotype of high FFA. However, as these experiments

progressed I found that I could no longer reproduce the FFA differences in wild type *vs. fld1Δ*. Eventually we learned that cell wall disruption by glass beads or enzyme digestion before lipid extraction abolished the difference in the amount FFA recovered in wild type and *fld1Δ* cells (Figure 10 B). Our initial results could have been caused by an effect of seipin on cell wall integrity in certain conditions leading to a more complete extraction of free fatty acids in seipin deficient cells. Consistent with this idea, I observed the difference of FFA level less often when the cells were grown to stationary phase when cell wall thickness is increased and perhaps a more equal extraction occurred [115].

Besides testing the importance of cell disruption for lipid extraction, I and others in the lab have tested several other steps of the lipid extraction protocol, which has led to improvement in the reproducibility of the results. We generally use chloroform/isopropanol (C/I) extraction (based on the plant protocol) but most yeast papers describe extraction with chloroform/methanol (C/M) [116]. Another difference between the protocols is the phase of the extraction that gets washed to removed impurities or yield more quantitative recovery. The C/I protocol was based on the Folch method [117], in which the organic phase of the lipid extraction is washed several times with 1M KCl to remove impurities. The C/M protocol, based on the Bligh and Dyer method [103], re-extracts the remnant solid pellet residue with chloroform. When I compared the two methods with two cultures of

wild type in two independent experiments, TAG was extracted equally, but SE and FFA were slightly more extracted by 12% and 10%, respectively, with the C/M method (Figure 10 C). The significance of these small differences are not clear. I conclude that even though the C/I protocol removes impurities from organic phase and the C/M protocol may increase yield, there was only a small difference, if any, in the efficiency of extraction between the two protocols.

We had been lysing cells using glass beads in a lysis buffer in Eppendorf plastic tubes prior to extraction with organic solvents, but published yeast protocols usually combined lysis and extraction in one step. However, I was worried about extracting the plastic of the tube, even though they seem to be resistant to organic solvents (i.e., they don't dissolve). Additionally, the amount of solvent in either protocol was too large for an Eppendorf tube, and samples would have to be split. For these reasons, we extracted after cell disruption. Another factor we considered was the extraction time. The plant protocol includes an overnight extraction with C/I after cell disruption, but many protocols online extract during cell disruption for only 10 to 30 minutes. Therefore, in a preliminary experiment I tested the amount of time for glass bead lysis (10 *vs.* 30 minutes) and for organic solvent extraction (10 minutes *vs.* O/N) with the C/M protocol (Figure 10 D). Time of lysis seemed to affect the amount of lipid extracted more than time of extraction. The sample from a thirty-minute lysis with overnight extraction contained the most lipid (determined by TLC), so I

normalized to that condition. A thirty-minute lysis with overnight extraction seemed optimal, with the most recovery over the other conditions in every lipid except sterol or DAG. I conclude that an overnight extraction is beneficial, but a thirty-minute lysis was more important. However, this experiment should be repeated to confirm these conclusions.

The final issue that affected the experiment-to-experiment variability besides the type of extraction was the loading of the lipids, dissolved in chloroform, onto the TLC plate. Because of the volatility of the solvent, our lab learned that results were more consistent and reproducible when equal volumes of sample were loaded. Quantification of lipids per unit cell weight or protein is then done after the quantification of spots (by densitometry) on the plate. Chloroform has low surface tension, and it tends to drip out of all pipettes. I obtained the best results when I quickly spotted 5 µl at a time on a plate. I believe quickly loading only multiples of five µl, or at least equal amounts, helps to minimize errors due to evaporation and loss of material.

This was a painful time of my doctoral work, but through these experiences, and help from Sungwon Han, our postdoctoral fellow, I learned how to test and develop a protocol. This period also taught me to trust my instincts since I never was happy with normalizing loading. Finally, I learned that each step of a protocol can make a difference in results.

3. Small Projects

A. Seipin deletion does not cause ER stress

Besides clusters of small droplets seen in *fld1Δ* yeast, our lab also found local ER proliferation creating droplet-ER tangles[2]. Considering the ER phenotype, I wanted to test whether seipin deletion caused either ER stress or made cells susceptible to agents that cause ER stress. My colleague, SungKyung Lee, in the lab had directly tested if *fld1Δ* yeast had increased *HAC1* (*XBP1*) splicing (an early event in ER stress is splicing of HAC1/XBP1 by the endonuclease IRE1) using Northern blotting, and found that there was no increase over wild type, indicating that ER stress did not accompany deletion of *FLD1* (unpublished results).

I then tested whether seipin deletion made yeast susceptible to ER stress. To this end I created an *ire1Δfld1Δ* mutant and tested survival with a titration of DTT and tunicamycin in wild type, *fld1Δ*, *ire1Δ*, and *ire1Δfld1Δ* yeast. Survival was measured as colony-forming units on rich plates. I treated the cells with different doses of drug, and plated equal amounts of cells in triplicate on rich medium plates. Survival of *fld1Δ* was similar to wild type except at the highest dose of tunicamycin, where the deletion strain appeared more sensitive. However survival of *fld1Δire1Δ* was clearly better than *ire1Δ* at multiple time points

(Figure 11). The *ire1Δ* strain had an extremely high colony count at a low dose of tunicamycin, and I believe there was a pipetting error when diluting the cells to plate them. Therefore, seipin deletion alone had little effect on ER stress, but the deletion may in fact protect cells from ER stress in the absence of *IRE1*. This was only shown with tunicamycin treatment, but DTT treatment had similar results (data not shown). These results should be confirmed since the experiment was just performed once.

B. The effect of different detergents on the seipin homo-oligomer

As described earlier, our lab showed that seipin is a homo-oligomer of about 9 subunits. However, a reviewer of the original submission of the manuscript questioned the use of a single detergent, Triton X-100, in our hydrodynamic experiments to determine the molecular mass of the oligomer. In response, we picked four other detergents with various properties: $C_{12}E_8$, another nonionic detergent; cholate, an anionic detergent; CHAPS, a zwitterionic (a positive and negative charge) detergent; and DDM (*n*-Dodecyl β-D-maltoside), a third nonionic detergent. All were used at a concentration above the critical micelle concentration. The three nonionic detergents had different micellar molecular weights: Triton X-100, 90 KDa; $C_{12}E_8$, 65 KDa; DDM, 50 KDa. Derk Binns and I performed the gradient centerfugations and immunoblotted the fractions from the gradients. We learned that different detergents affected the

apparent molecular weight (AMW) of the complex (Figure 12 A), and we found that the effect on the AMW was inversely related to the partial specific volume (Figure 12 B). Therefore, the less dense/more buoyant the detergent was, the smaller the AMW (towards 200 KDa). Conversely, since partial specific volume is the inverse of density, the more dense the detergent, the larger the AMW (approaching 400 KDa). In conclusion, the density or buoyancy of the detergent affected the AMW more than it affected the apparent number of monomers in the complex. Since DDM is an outlier on the curve, it may also alter the number of monomers in the seipin homo-oligomer. Another intriguing possibility is that it helps to stabilize a binding partner of the oligomeric complex.

C. Seipin deletion alters the protein composition of lipid droplets

Since our lab believes that seipin deficient droplets are probably ectopic and dysfunctional, we have been trying to define how they are dysfunctional. One of the ways might be reflected in an altered protein composition. To test this possibility, I prepared highly purified lipid droplets from wild type and *fld1Δ* yeast, removed the lipids, subjected the proteins to SDS-PAGE, and stained the resulting gel with silver. I found slight differences in protein composition (Figure 13). In three different purifications, a band around 57 KDa and a band about 24 KDa decreased in *fld1Δ* cells, and a band at 22 KDa increased in *fld1Δ* cells. In two of the three purifications, a band at 30 KDa increased in *fld1Δ* cells. A

collaborator, (Karin Athenstaedt, Graz, Austria), also found the decrease of bands at 33 and 35 KDa in *fld1Δ* cells that could represent my band at 24 KDa, although the large molecular weight differences in the two labs make this possibility unlikely. She found only a very slight decrease, as I did, of a band at 57 KDa (except perhaps a very slight decrease). She identified the band around 34 KDa that was decreased in intensity in *fld1Δ* to be Ayr1p, a NADPH-dependent 1-acyl dihydroxyacetone reductase, involved in PA synthesis. It reduces a ketone group on 1-acyl dihydroxyacetone to an alcohol (LPA) so that a second acyl chain can be added at the SN2 position to make PA. It is possible that this reduction of Ayr1p on *fld1Δ* LD causes the elevation of cellular PA seen by Fei *et al*., if there is more substrate in ER or the enzyme is more active in the ER. Dr. Athenstaedt did not see any bands increase in *fld1Δ* yeast, but she also found a moderate decrease in Erg7p and a slight decrease in Erg6p, enzymes involved in ergosterol synthesis.

D. Lipid droplet biogenesis may be a two-step process (in cells with seipin deleted)

In a few of the images of *4KOfld1Δ* yeast, I observed three novel morphologies. Most prominent was that several of the small lipid droplets (100 nm) were more grey than white, but they definitely had a phospholipid border

(Figure 14, chevrons). This could signify that the phospholipid layer is created before neutral lipid is packaged into droplets, which might be captured in *4KO* yeast at an early time point of *DGA1* expression. But this may also indicate cytoplasm above or below the droplet in the thin section, which would be more likely with tiny droplets. I also saw several lens-like structures connected to membranes such as those labeled by arrows in Figure 14. Finally, in Figure 14 C, I captured a circular organelle from which droplets seemed to be emanating. Have I captured LDs in the process of normal biogenesis or in the process of lipolysis by a peroxisome, or is this phenomenon very specific for *4KOfld1Δ* yeast in galactose medium only expressing *DGA1*? I am inclined to think that *4KOfld1Δ* (and probably *fld1Δ*) droplets are "younger" than normal droplets. Are seipin droplets less mature, or just smaller? These are questions that could be addressed in the future.

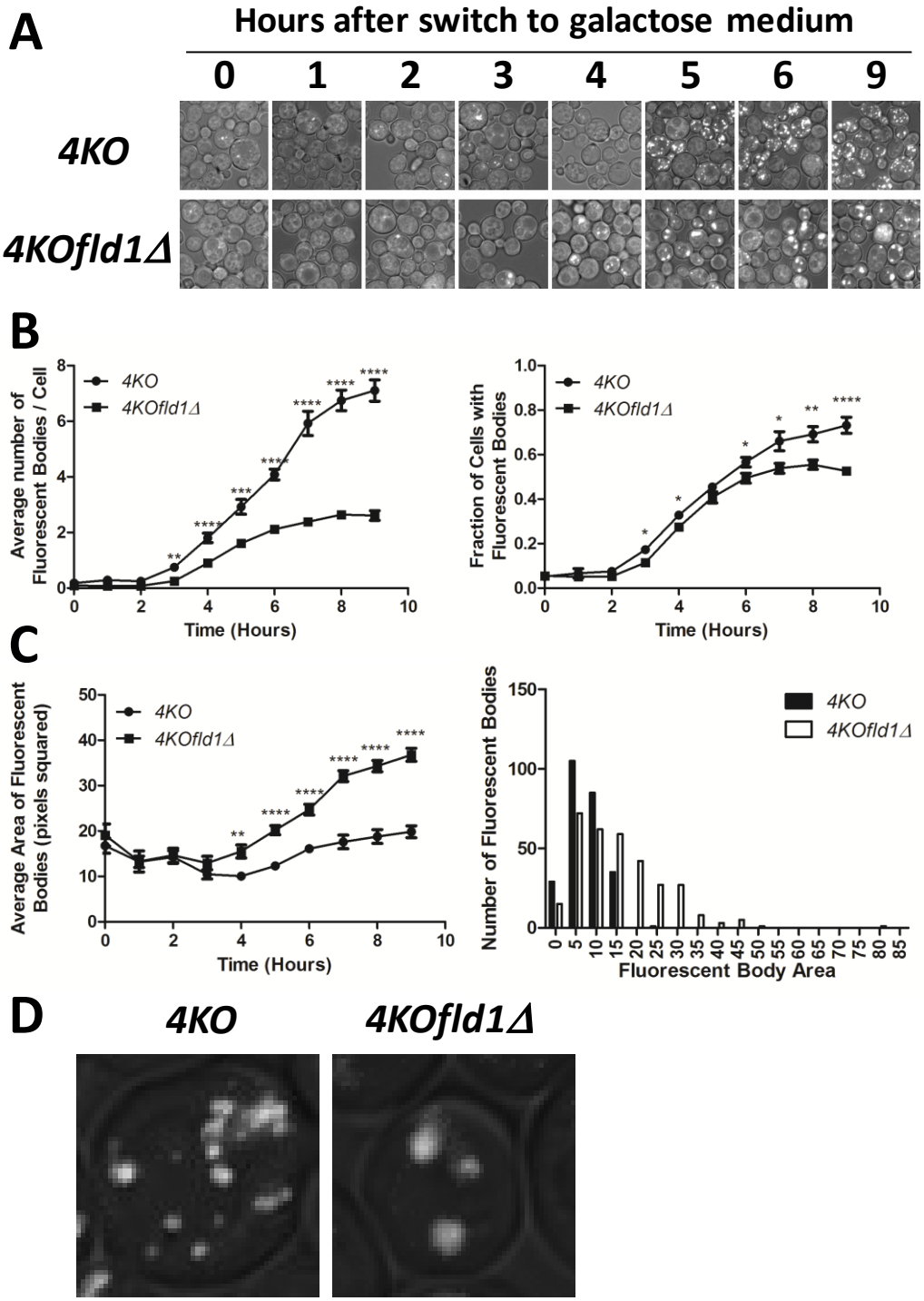

Figure 6. Seipin deletion alters lipid droplet biogenesis of triacylglycerol droplets. (A) Representative images of *4KO* and *4KOfld1Δ* cells expressing galactose promoter-driven *DGA1* on a plasmid at different hours after dilution into galactose medium (time zero is in raffinose medium before switch to galactose).

Cells were stained with BODIPY. (B) Quantification of four time courses as described in A. Fluorescent bodies and the fraction of cells in a field with FB were counted and plotted versus time. Left panel shows the average number of FB per cell. Right panel shows the fraction of cells with at least 1 FB. Three fields per time point, 4 experiments. (C) FB area was quantified with ImageJ and plotted versus time. Left panel quantified FB area in fields of cells. Right panel quantified 20 FB per field at 5 hours after switch to galactose medium. (D) Close-up images of single cells from panel A, 6 hours. For panels B and C *: p-value <0.05, **: p-value <0.01, ***: p-value <0.001, ****: p-value < 0.0001. Error bars are standard error of the means.

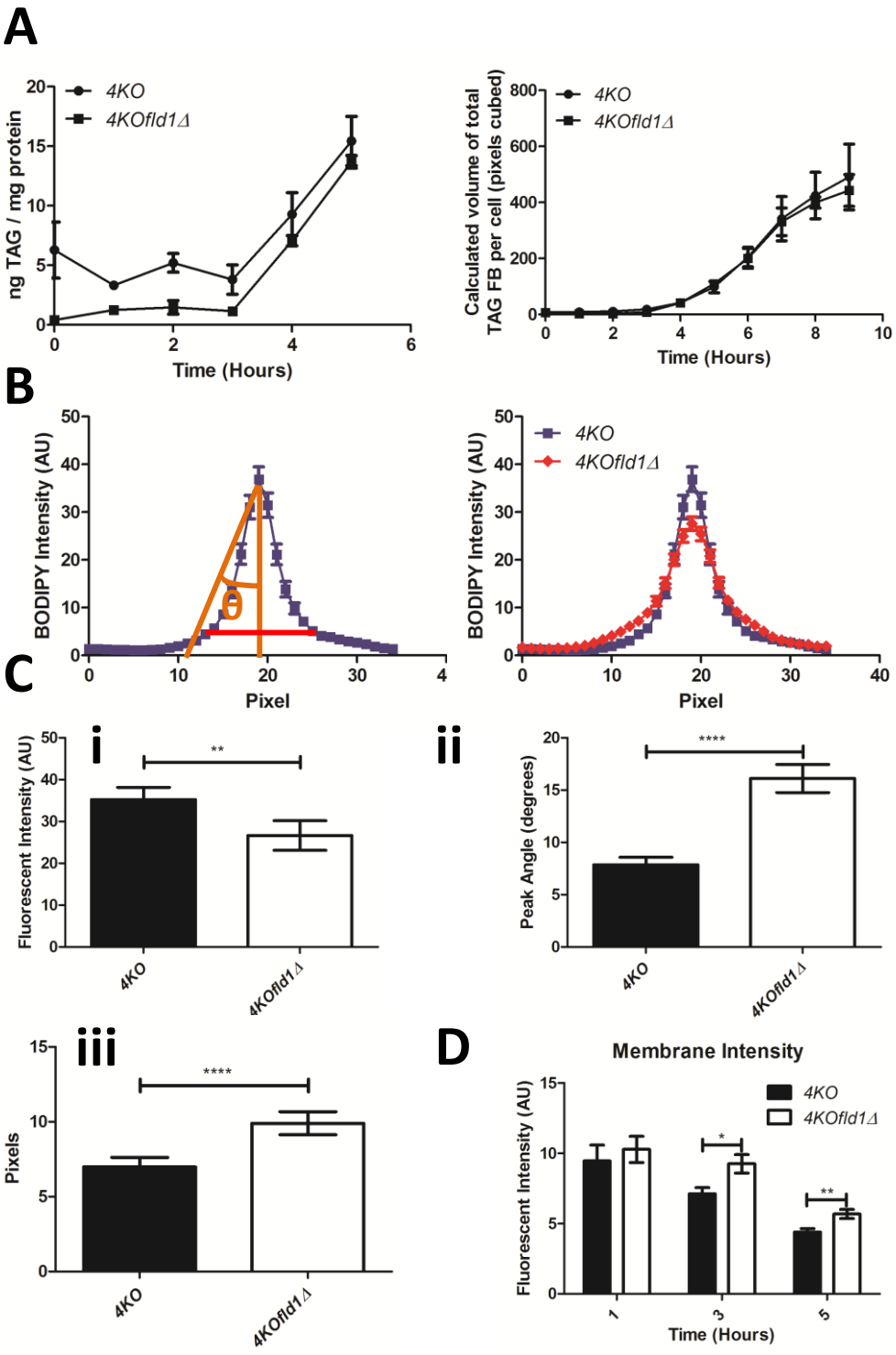
A
4KO
4KOfld1Δ
ng TAG / mg protein
Time (Hours)
Calculated volume of total TAG FB per cell (pixels cubed)
Time (Hours)
B
BODIPY Intensity (AU)
θ
Pixel
4KO
4KOfld1Δ
BODIPY Intensity (AU)
Pixel
C
i
Fluorescent Intensity (AU)
**
4KO
4KOfld1Δ
ii
Peak Angle (degrees)
****
4KO
4KOfld1Δ
iii
Pixels
****
4KO
4KOfld1Δ
D
Membrane Intensity
4KO
4KOfld1Δ
Fluorescent Intensity (AU)
*
**
Time (Hours)

Figure 7. Seipin deletion inhibits early TAG formation, integrity of fluorescent bodies, and possibly TAG packaging. (A) Results from thin layer chromatography of lipid extracts from *4KO* and *4KOfld1Δ* cells expressing DGA1 behind a galactose-inducible promoter quantified using densitometry of acid-charred plates. Results from two independent experiments. (B) and (C) Characterization of line scans of FB in *4KO* and *4KOfld1Δ* cells that resulted in peaks of BODIPY intensity over distance. Twenty FB per field of three fields from three independent experiments were characterized at 5 hours after switch to galactose medium. The left panel of (B) is an illustration showing the peak width in red and the peak angle, theta, in orange. The right panel of (B) shows the averages of fifty-two peaks for each strain aligned at the highest intensity pixel. Panel (C-i) characterizes intensity above background in arbitrary units (AU). Panel (C-ii) characterizes peak angle, theta, in degrees (See methods for more detail). Panel (C-iii) characterizes peak width in pixels at the inflection point as indicated in (B) left. (D) BODIPY intensity was quantified as in (B), but for intracellular membranes. See Figure 6 for explanation of asterisks.

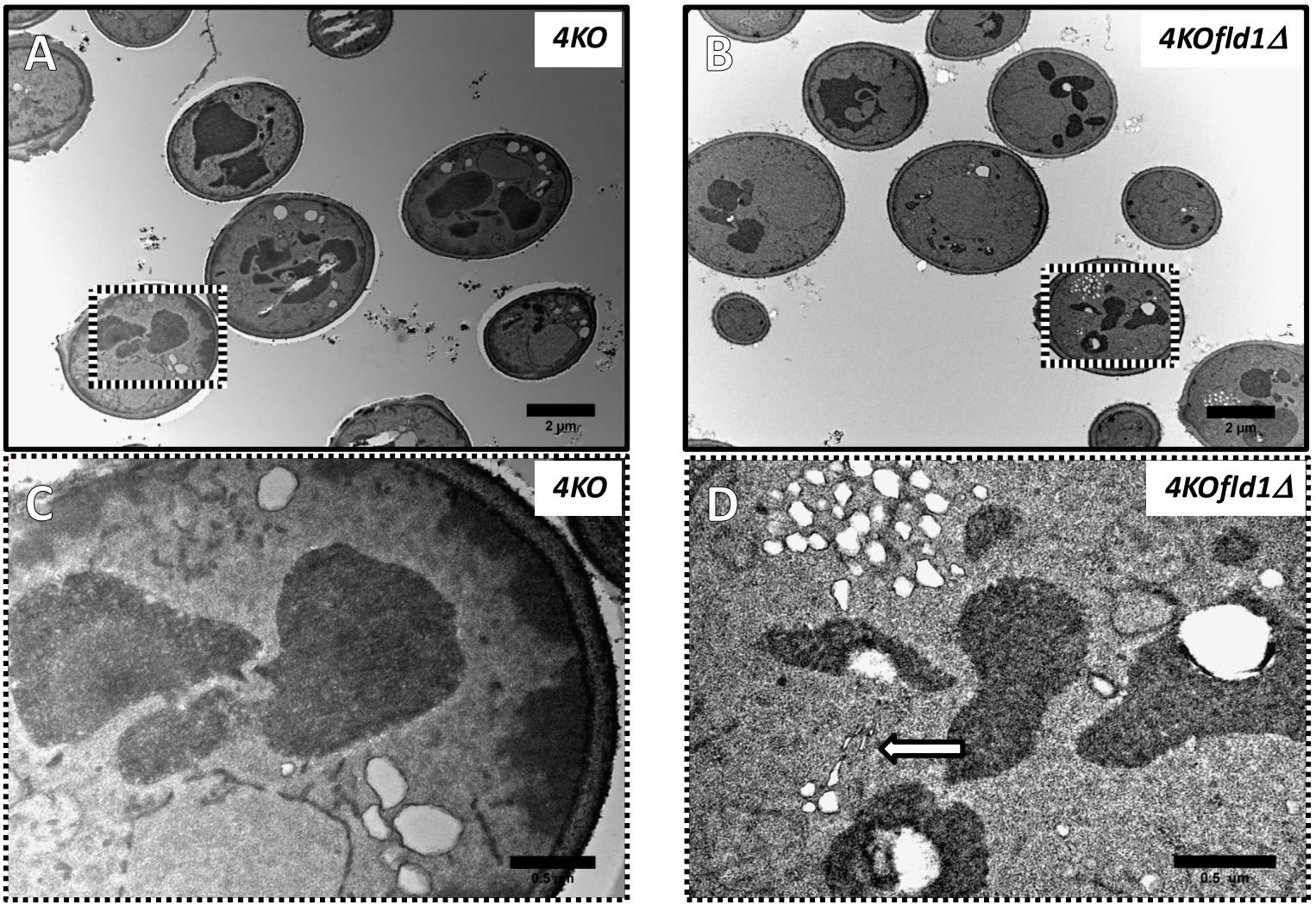
A
4KO
2 µm
B
4KOfld1Δ
2 µm
C
4KO
0.5 µm
D
4KOfld1Δ
0.5 µm

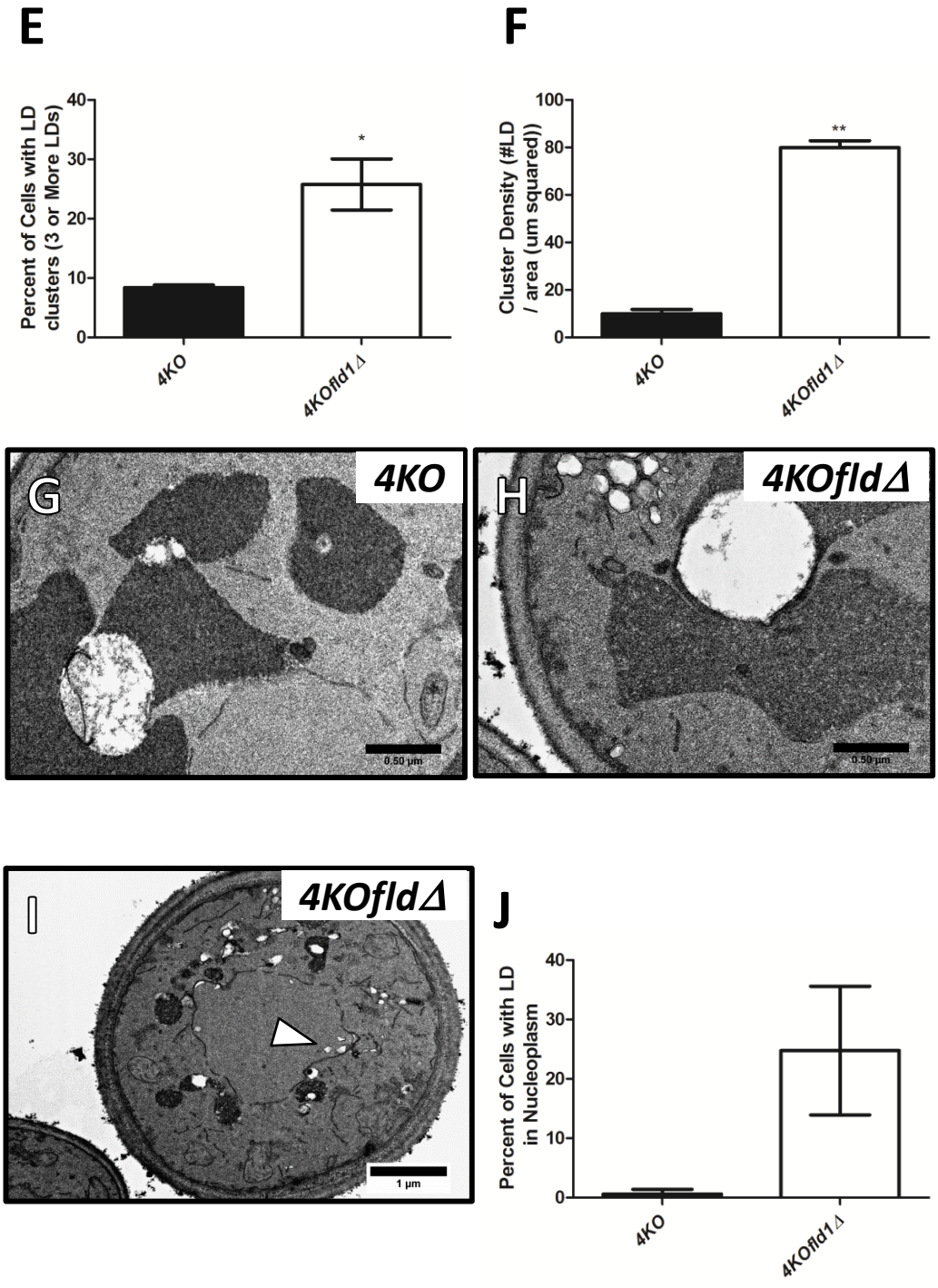
E
Percent of Cells with LD clusters (3 or More LDs)
40
30
20
10
0
*
4KO
4KOfld1Δ
F
Cluster Density (#LD / area (um squared))
100
80
60
40
20
0
**
4KO
4KOfld1Δ
G
4KO
0.50 µm
H
4KOfldΔ
0.50 µm
I
4KOfldΔ
1 µm
J
Percent of Cells with LD in Nucleoplasm
40
30
20
10
0
4KO
4KOfld1Δ

Figure 8. Seipin deletion decreases TAG droplet size and induces droplet formation in nuclei. (A) and (B) Representative images of cells at 10,000X in the indicated strains expressing *DGA1* behind a galactose-inducible promoter and fixed at 6 hours after switch to galactose medium. Scale bar, 2 μm. Striped boxes indicate the area shown in the high magnification images below (C) (50,000X) and (D) (60,000X). Bar in striped boxes, 500 nm. Arrow indicates lens-like structures (or flat LD). (E) Quantification of the percentage of cells containing LD clusters (a minimum of three cells within ~200 nm of each other. (F) Characterization of the density of droplets in clusters from *4KO* and *4KOfld1Δ* cells. (G) and (H)- Images illustrating large electron sparse structures that are usually associated with vacuoles in both *4KO* (G) and *4KOfld1Δ* (H) yeast. Scale bar, 500 nm (60,000X). (I) An example of droplets in the nucleoplasm of *4KOfld1Δ* cells (indicated by an arrowhead). Scale bar, 1000 nm (20,000X). (J) Quantification of percentage of cells with LD in nuclei in both strains expressing Gal-*DGA1*. See Figure 6 for explanation of asterisks.

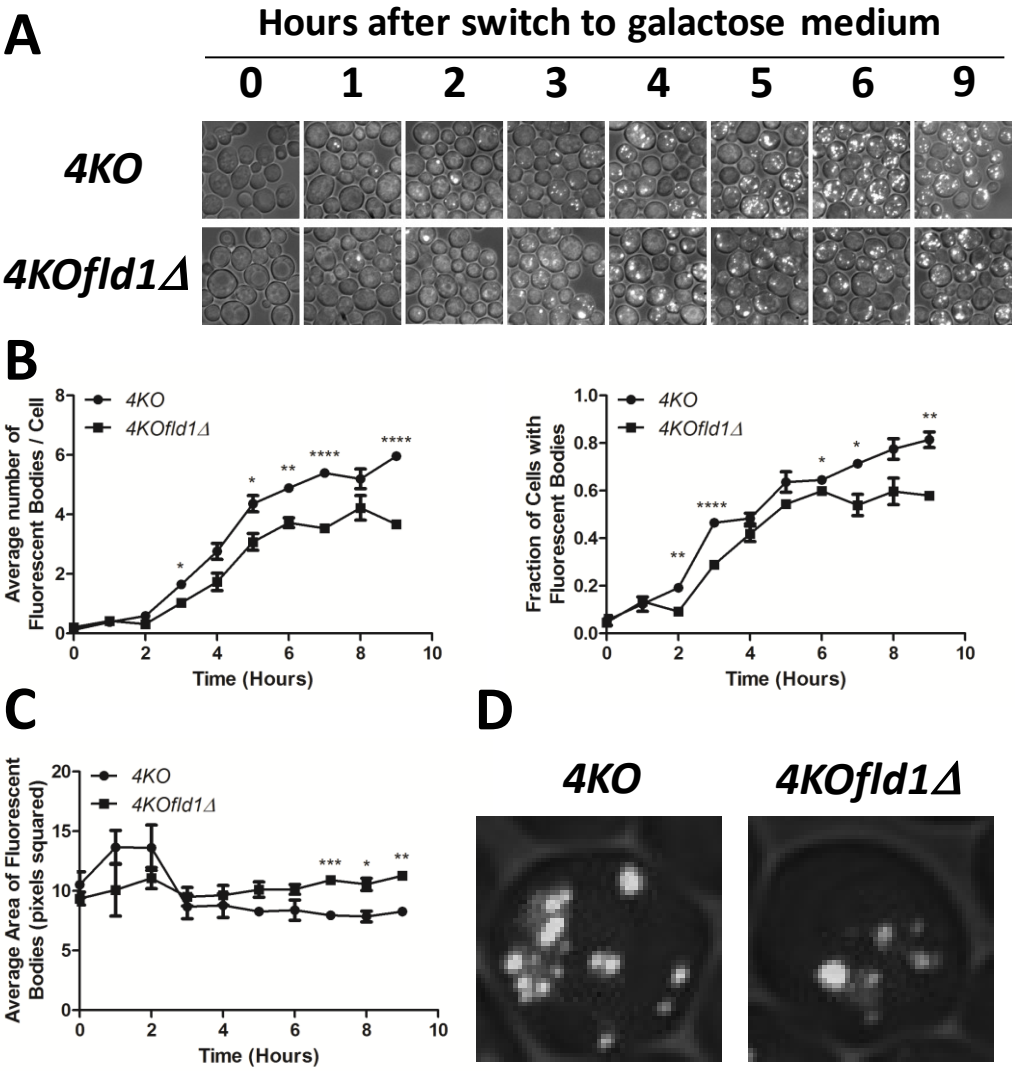

Figure 9. Seipin deletion modestly affects SE fluorescent body formation. (A) Representative images of *4KO* and *4KOfld1Δ* cells expressing galactose promoter-driven *ARE1* at different times after switch to galactose medium (time zero is in raffinose medium immediately before switch to galactose). Cells were stained with BODIPY. (B) Quantification of one experiment performed as in (A) (including 7 and 8 hours after switch to galactose medium). Fluorescent bodies and the fraction of cells in a field with FB were counted and plotted versus time. Left panel shows the average number of FB per cell. Right panel shows the fraction of cells with at least 1 FB. Three fields per time point, 1 experiment. (C) Area of FBs were quantified with ImageJ and plotted versus time. (D) Close-up images of single cells from panel A, 6 hours. See Figure 6 for explanation of asterisks.

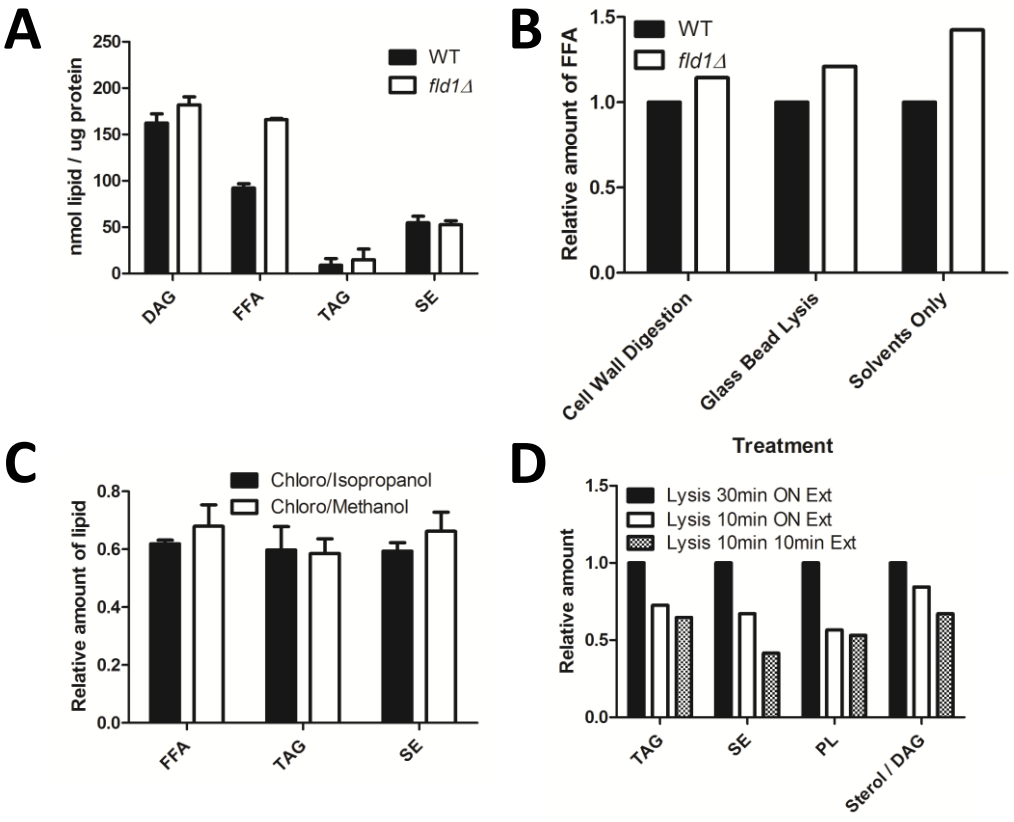

Figure 10. Effects of seipin deletion on neutral lipid levels based as measured by variations of lipid extraction protocol. (A) Whole cell neutral lipid concentration in minimal medium during log-phase growth in WT and *fld1Δ* quantified from acid-charred thin layer chromatography plates. DAG, diacylglycerol; FFA, free fatty acids; TAG, triacylglycerol; SE, steryl-ester. Cells were extracted using the chloroform/ isopropanol method (see Methods for more details). (B) FFA levels from a single experiment expressed as a percentage of WT that were quantified as in A. Treatment indicates the method used to disrupt the cell wall before solvents were added for lipid extraction. (C) Lipid levels from WT cells using two different extraction methods, chloroform/methanol and chloroform/isopropanol, expressed as a percentage of standard (40 µg of triolein (TAG), 30 µg of oleic acid (FFA), or 50 µg of cholesteryl oleate (SE)). Results from two experiments with duplicate cultures. Error bars are standard error of the means. (D) Difference in relative lipid levels comparing two different lysis times (30 minutes *vs.* 10 minutes) and two different extraction times (overnight *vs.* 10 minutes) that are expressed as a percentage of 30 minute lysis with overnight extraction. Results from a single experiment.

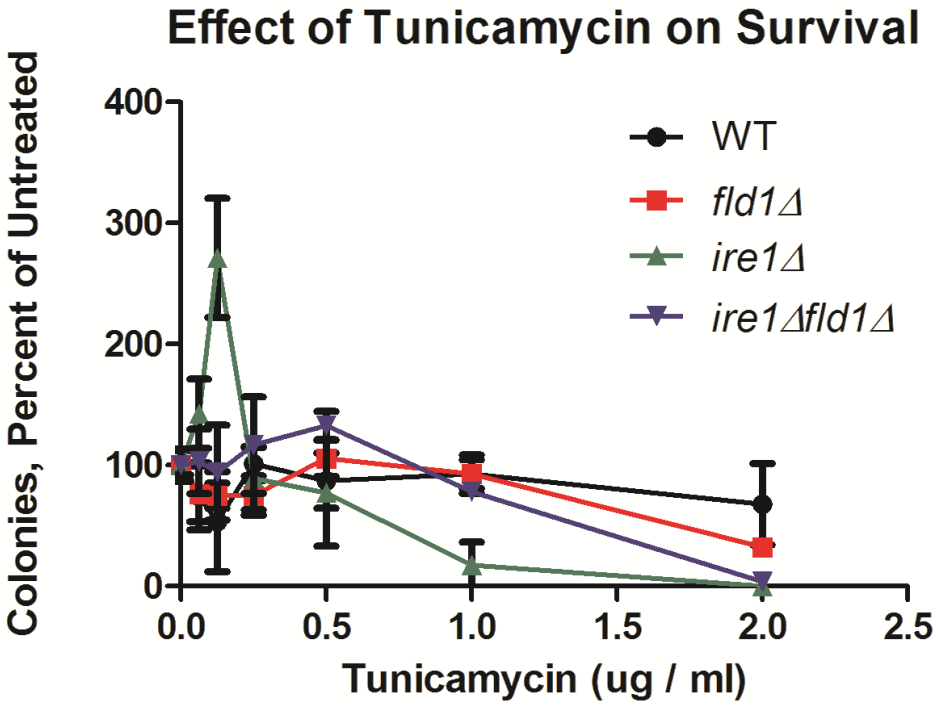

Figure 11. Seipin deletion does not seem to enhance susceptibility to death due to ER stress. Survival curve of the indicated strains with increasing doses of tunicamycin. Equal cells were plated in triplicate after 30 minute treatment with drug. Colony numbers were counted after two days of growth and expressed as a percentage of untreated cells. Results are a single experiment plated in triplicate. Error bars are standard error of the means.

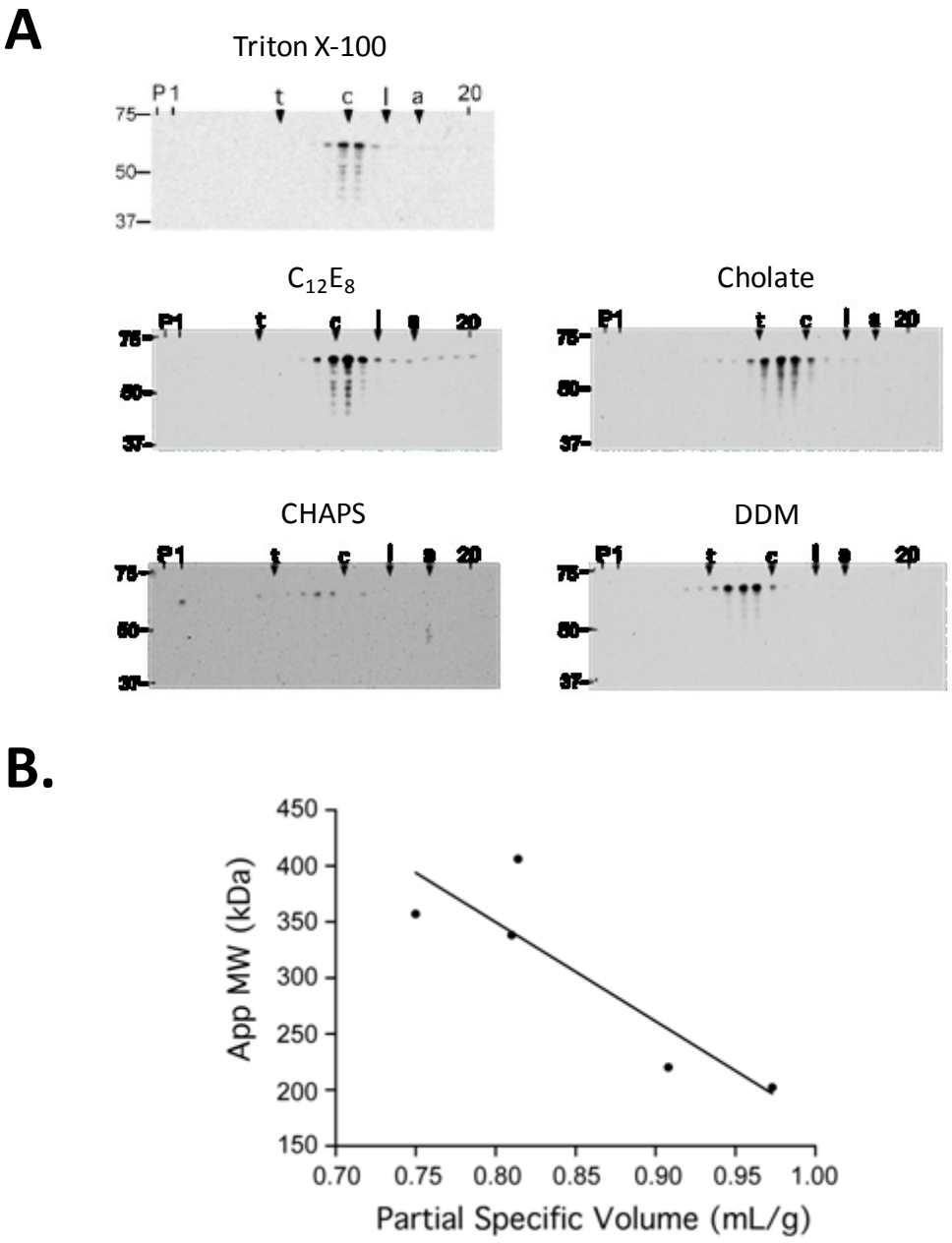

Figure 12. Effect of different detergents on the seipin homo-oligomer. (A) Detergent glycerol gradients of crude membrane preparations solubilized in the same detergent from cells expressing seipin-13xmyc fusion protein from the genome were fractionated and immunobloted for myc. Apparent molecular weight was calculated using the standards: t, thyroglobulin (669 KDa); c, catalase (232 KDa); l, lactate dehydrogenase (140 KDa); a, albumin (67 KDa). (B) The correlation between apparent molecular weight of the seipin oligomer in each detergent from A and the partial specific volume of those detergents. Figure and legend

reproduced in part from Figure 1 and Supplemental Figure 2 of **Binns, D., Lee, S., Hilton, C.L., Jiang, Q.X. & Goodman, J.M. Biochemistry 49, 10747-10755 (2010).**

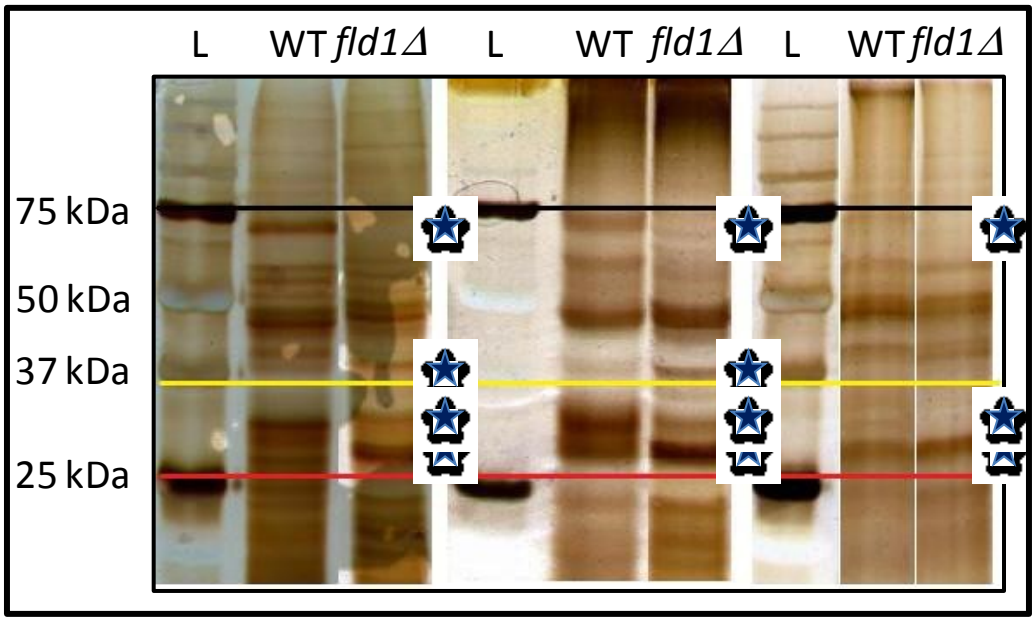

Figure 13. Seipin deletion alters the protein composition of lipid droplets. Lipid droplets were purified by separation on density gradients (see Methods). The purified droplets were de-lipidated with ether, subjected to SDS-PAGE, and the gel was then silver stained. Three independent preparations are aligned and shown. L indicates ladder of protein standards. Blue stars to the right of lanes indicate changes between WT and *fld1Δ* that appear at least twice.

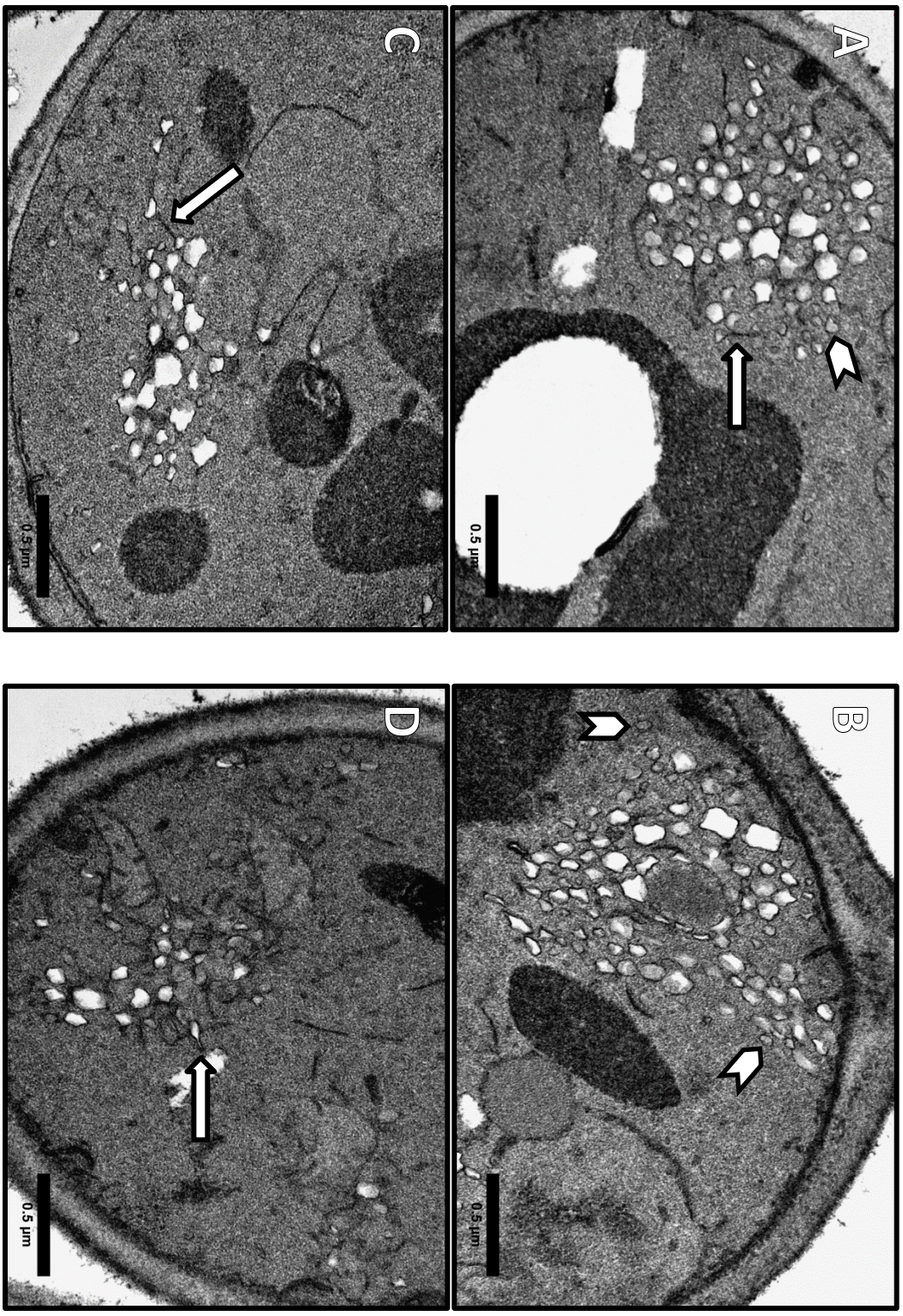
A
0.5 µm
C
0.5 µm
B
0.5 µm
D
0.5 µm

Figure 14. *4KOfld1Δ* clusters have evidence of lens-like, flat droplets in communication with membranes and phospholipid-defined, medium electron density droplets. (A-D) Samples processed as in Figure 3. Images shown are 60,000X. Bar, 500 nm. Arrows indicate lens-like droplets or membranes from which droplets appear to be emanating. Chevrons indicate droplets of medium electron density droplets within a membrane.

Discussion

Summary

The results are clear that seipin is involved in lipid droplet biogenesis, at least in our system. Fluorescent body number and size were oppositely affected (number down, area up) in *4KOfld1Δ* yeast, as well as the integrity and regularity of FB, but in the electron microscopy images, we learned that mutant FB were actually clusters of small droplets at least at 6 hours after switch to galactose medium. My data regarding the effect of seipin on whole cell triacylglycerol levels during induction were inconclusive, but later work with chromosomally integrated GAL-*DGA1* showed that levels of TAG were very similar with or without seipin during induction. I also have presented fluorescence data of BODIPY-stained intracellular membranes suggesting that there is more TAG in membranes. Finally, steryl-ester fluorescent body formation (driven by plasmid-encoded GAL-*ARE1*) is inhibited in *4KOfld1Δ* yeast, but to a lesser extent than during TAG FB formation.

In several side projects, I leaned about protocol development and troubleshooting, a possible role of seipin in droplet protein composition, the effects of different detergents on the seipin homo-oligomer, and the lack of a role

for seipin in ER stress. Lipid yields were extremely affected cell lysis and extraction conditions. However, there was little difference of isopropanol *vs.* methanol in the extraction solvent or in different secondary extraction conditions. Regarding droplet protein composition, seipin deletion resulted in some differences in stained bands from SDS-PAGE, but not much reproducibility between my and Dr. Athaenstadt's preparations except possibly a reduced amount of Ayr1p. Different detergents had an effect on the apparent molecular weight of the seipin homo-oligomer-detergent complex without changing the mass of the oligomer, with the possible exception of *n*-dodecyl β-D-maltoside. Seipin deletion did not cause an increase in the ER stress reaction of *HAC1* splicing or susceptiblity to tunicamycin, indicating that *fld1Δ* cells did not display an increase in ER stress. Finally, EM images of *4KOfld1Δ* yeast seemed to depict lipid droplet structures suggestive of the lens model of biogenesis, with the caveats that the droplets store only TAG, and the lens droplet morphology was only observed in a strain lacking seipin.

Future Directions

The immediate goal of creating the biogenesis system was to have a tool to see if seipin was involved in lipid droplet biogenesis or if it was involved in some downstream maintenance pathway that kept LD normal, and we learned that

seipin is involved in both TAG and SE droplet biogenesis. Specifically, we know seipin is involved with TAG droplet architecture, since a large majority of LD are nanoLDs (100 nm in diameter) and yet there is equal whole cell TAG. How directly seipin is involved in lipid droplet biogenesis is still a mystery.

I believe seipin may be a structural component of the ER-droplet sub-domain, but it is not a coat protein like a COPII component or a perilipin since it localizes to ER and not droplets. If seipin were a valve, it could explain why droplets are smaller and there is more lipid in membranes (assuming this is reflected in my staining measurements) because without the valve, lipid would freely flow back into ER, decreasing the volume of lipid in droplets. How would such a valve operate at the molecular level? If the lumenal loop of seipin is amphipathic enough to exist in a hydrophobic environment (it binds tightly to membranes when expressed by itself (Hilton, Han, and Cartwright, unpublished observation)), then the N- and C-tails could still be in the cytoplasm and the rest of the protein could be completely "submerged" in the neutral lipid in the "neck" of the droplet, such that the interior of the toroid oligomer (transmembrane segments and loop) is in the neck while the termini face the cytosol. This orientation would put the toroid in the right location relative to ER and LD during droplet formation and maintenance. This orientation is doubtful, however, because the toroid would have to rotate or alter shape so that the termini remain in the cytosol and the loop returns to the inner leaflet of the lumen of the ER, when

the seipin toroid is "free" of a droplet. The seipin toroid could still surround the neck with the previous predicted topology [50] during droplet formation and maintenance, such that the cytoplasmic tails surround the neck, but this places most of the protein in the leaflets of the ER distal to the droplet. On top of that, a physical neck of a droplet with respect to the ER has not been observed. An additional unknown issue is whether seipin acts as a one-way valve or a two-way channel. Could the toroid exclude lipid with charge or a hydrophilic face (e.g., bound to water)? Could it let non-neutral substrates in but keep neutral lipid out of the plane of the ER?

What evidence would we need to show seipin functions as a valve? One way is to definitively show that there is more neutral lipid in membranes in seipin-deficient cells. To this end our lab is currently measuring the density of ER by isopycnic sucrose gradient sedimentation in *3.5KO* and *3.5KOfld1Δ* yeast (see below), since membranes with more lipid should float higher in the gradient. In my system, we encoded GAL-*DGA1* on a plasmid, but we later knocked-in the GAL1-10 promoter in front of the *DGA1* open reading frame in the genome in a triple deletion background to get more homogenous control over *DGA1* expression (referred to as the 2nd generation; my plasmid system described in this dissertation was the first generation). In this second generation, the background strain is referred to as *3.5KO*, and the *fld1Δ* strain as *3.5KOfld1Δ*. Preliminary

experiments indicate that *3.5KOfld1Δ* cells expressing *DGA1* have relatively more TAG in the ER and "cytosol" compartments and less in the LD fraction. TAG in the cytosol may indicate that nano-droplets that do not contain enough lipid, or are two small, to float all the way to the top during centrifugation.

If lipid precursors bind to seipin, this may suggest that seipin could channel the precursors. In this regard, we observed in the lab that seipin bound to several phosphorylated phosphatidyl inositol species, but not neutral lipid. As a valve, however, it should repel neutral lipid from one side. If neutral lipid is required for, or enhances, oligomerization or conformation of seipin, I think this could indicate that seipin is regulated by neutral lipid. Testing this hypothesis will require structural studies with purified seipin. If a region were to be identified that were a candidate for valve function, it may be possible to engineer a seipin that was directionally reversed (assuming a one way valve), that should block LD formation, since no lipid would be able to go into a droplet, just "out".

Another way seipin could be promoting formation of larger droplets is by regulating lipolysis. An increase in lipolytic activity without block of *de novo* lipid synthesis results in many small droplets (perhaps to prevent lipotoxicity) [118], which is what we mainly see in our biogenesis system in *4KOfld1Δ* yeast. It would also make sense that both supersized droplets and membrane wrapping

would be mechanisms to prevent increased lipolysis by physically limiting access to lipase. The effect on neutral lipid by increased lipolysis may be counteracted with over-expression of DGA1 in my system (*4KO*) and that with the chromosomally-expressed DGA1 construct (*3.5KO*). In this regard, measuring lipolysis (by glycerol release) during DGA1 induction should be informative. It is possible we may not see a difference if the glycerol is efficiently being recycled into lipid at the same time, so we may have to switch yeast back to glucose medium that would truncate *DGA1* expression and activity. Conversely, adding a lipase inhibitor may rescue the large FB phenotype. Since the only lipase inhibitors available are active against pancreatic lipases [119], we would have to determine if these inhibitors were active towards yeast lipases. We can also knock out the lipases in our biogenesis system although the lack of auxotrophies and antibiotic-resistance markers in our multiply-deleted strains may limit this approach. If these results become feasible, we can see if Fld1p interacts with any of the lipases or if some post-translational modification of one of the lipases is changed in *fld1Δ* yeast. Indeed, the TAG lipase Tgl3p requires Fld1p for efficient targeting [63].

A third way seipin can alter LD size without altering TAG levels is by altering the protein composition of the LD. Perhaps this alters the coat of a droplet or actually decreases fusion of nanoLD, although *in vitro* data implies that seipin

null droplets are actually fusogenic [60]. How seipin maintains protein composition is harder to explain. It could possibly help import certain proteins onto the lipid droplet, or it could just help maintain the ER-LD junction. If seipin were involved in protein import or junction maintenance, I would expect to see a larger defect in LD protein composition. However, if this were the case, over-expression of LD proteins might rescue the localization of some of these proteins as well as the LD morphology phenotype. But levels of droplet protein mRNA do not change in *fld1Δ* [62]. A complementation screen may be useful, or even overexpressing proteins deficient in droplets from *fld1Δ*, such as Ayr1p, Erg6p, and Erg7p from Dr. Athenstaedt's LD proteome work. Additionally, the complementation screen may uncover other functions of seipin.

There are other questions I would like to answer in the biogenesis system. As discussed earlier, localized ER proliferation and supersized droplets are seen in *fld1Δ* cells but not in our *de novo* droplet system. It would be interesting to see if membrane wrapping and/or supersized droplets were a product of LD "age", presence of steryl-ester, a balance of phospholipid to neutral lipid (which could be altered directly by *LRO1*, the other DAG acyltransferase), or a specific culture medium (± phospholipid precursor head groups such as Fei found [62]). I would, therefore repeat the electron microscopy study with *ARE1* and *LRO1* (and *DGA1*) in *3.5KO* and *3.5KOfld1Δ* cells alongside WT and *fld1Δ* control strains. This may

be an overzealous plan, but it should prove definitive in addressing clustered *vs.* supersized droplets and membrane wrapping of LDs. An additional observation I made was the presence of lens-like small droplets in the *4KOfld1Δ* strain. To determine if these structures are only found in *fld1Δ* strains, a more robust examination at the electron microscopic level of the 4KO strain during droplet biogenesis should be undertaken. We performed electron microscopy on cells fixed at T6, and another group imaged cells at T0 and T4 [89], but what do these droplets look like at very early times of TAG or SE synthesis? Do we see medium electron-density droplets bound by a phospholipid layer (assumed to be a monolayer)? Do we see lens-like or flat droplets like we do in *4KOfld1Δ* cells? Do we ever see a "neck" between LD and ER? We hope that our system can answer some of these basic questions of LD biogenesis.

An additional issue is the modest effect of *FLD1* deletion on droplet formation driven by *ARE1* compared to *DGA1* (Figure 6 *vs.* Figure 9)? I hypothesize that increased sterol in cells expressing GAL-*DGA1* compared to those expressing GAL-*ARE1* (which is converting sterol to steryl-ester) could make membranes more stiff and increase the intra-bilayer pressure that has to build up to sprout ectopic droplets (such as those I see in the nucleoplasm). One way to test this is to add excess sterol to *3.5KO* and *3.5KOfld1Δ* cells expressing

ARE1 to determine whether the phenotype becomes more pronounced and resembles the GAL-*DGA1* system. There may be a problem with the experiment, however, if the increasing Are1p activity during the induction can convert the exogenous sterol to the ester. Hopefully we can saturate the enzyme with a titration of sterol. Another way would be to extract ergosterol from cells expressing *DGA1* possibly with methyl-β-cyclodextrin (previously shown to be effective in yeast [120]). Cyclodextrin is usually used to extract sterol from plasma membranes, but presumably the remaining sterol would re-distribute throughout the cells, thereby decreasing the effective concentration in ER membranes. A decrease in ER sterol would have to be confirmed biochemically. This experiment should show whether the phenotype becomes less pronounced in *3.5KOfld1Δ* yeast.

Another possibility to explain the less pronounced size phenotype in *ARE1* expression compared to *DGA1* in the absence of seipin is that steryl-ester clusters are smaller and closer to *3.5KO* (and in my case, *4KO*) steryl-ester LD size due to the chemical nature of steryl-ester or the size of the pool of steryl-ester that cells maintain. I believe this may be true because my data indicate that *4KO* SE FB are smaller than *4KO* TAG FB, and I assume that the difference in *fld1Δ* droplets are proportional. It is not possible to compare SE and TAG (*4KO*) FB size based on my graphs because the size was quantified differently: TAG FB area is from raw

ImageJ data regardless of morphology. For the SE data when an FB appeared to be a cluster, the individual smaller droplets were counted separately (compare Figure 6 C and Figure 9 C). The raw data is saved, so a direct comparison can be performed, and SE FB in *4KO* cells are generally smaller than TAG FB. Therefore, it is probable that the *4KOfld1Δ* droplets in the SE clusters are smaller as well, and EM analysis of our two strains expressing *ARE1* at T6 could show this. It seems likely that *4KOfld1Δ* SE droplets are small enough to decrease the area of *4KOfld1Δ* FB (probably representing LD clusters).

The cause of the smaller effect of *fld1Δ* on SE *vs.* TAG droplets, however, is probably more complicated than simply a smaller LD area. There may be an organizational difference within clusters in the *4KOfld1Δ* in the two droplet types. The number of FBs per cell differs (in the presence of seipin), with SE FBs reaching 6.0, while TAG FBs peak at 7.1. In *4KOfld1Δ* cells, SE FB number/cell peaks at 4.2, but TAG FB number/cell peaks at 2.6, which does not correlate with the corresponding values in the presence of seipin. This does not preclude the possibility that *4KOfld1Δ* clusters composed of SE have fewer droplets than those composed of TAG due to decreased tethering among droplets, for example. (We would need EM evidence to test this difference in nanoLD density.) Perhaps

hypothetical tethering proteins insert less efficiently into SE droplets than TAG droplets, and an examination of LD proteins in both strains expressing either *DGA1* or *ARE1* may reveal this. In summary, the decrease in area phenotype we see with SE FB could be directly related to droplet volume in *fld1Δ* cells based on lipid species or a change in organization of *4KOfld1Δ* clusters (fewer droplets per cluster and more clusters).

With more time, I would also further validate the conclusions drawn from some of my data, mainly by quantifying more trials with *ARE1*, re-characterizing *DGA1* FB area by correcting the raw data, and a third trial of lipid levels in the *DGA1*-induction experiment.

Even if over-expressing Ayr1p, Erg6p, or Erg7p, proteins that were under-represented in the LD proteome studies by Karen Athenstaedt do not rescue the FB phenotype, I still believe they should be investigated. First, I would see if a difference in localization of CFP (or mCherry) fusion proteins (with green BODIPY staining) can be visually distinguished between WT and *fld1Δ* cells to further show that there is a difference in LD localization and to possibly track the re-localization in another compartment of the cell. I think the degradation rates of these proteins should also be measured in WT and *fld1Δ* cells to see if the rates are higher in *fld1Δ*, which could explain their decrease in LD localization in the

seipin mutant. Since continue to search for binding partners of seipin, direct co-immunoprecipitation should be tested between Fld1p and these proteins.

Conclusion

I am the first to show definitive evidence for seipin being involved in LD biosynthesis which is different from effects on adipogenesis in professional mammalian adipocytes. I also show evidence that there is more TAG in membranes of *4KOfld1Δ* cells, suggesting that seipin may work as a valve to regulate packaging. Finally, I provide the first evidence that nascent TAG droplets in galactose minimal medium do not have membrane wrapping or supersized droplets, and that nanoLDs have lens like structures and perhaps "half-filled" LD. This may lend clues to the general molecular function of seipin apart from (or connected to) its role in pre-adipocytes as they transition to adipocytes. Knowledge of seipin's role in biogenesis may have broader applications. The biogenesis system allows study of early versus late defects in seipin-deficient droplets such as proximal membrane wrapping and perhaps alterations of lipolysis. Finally, I was able to quantify FB area using a combination of computer software and human correction, optimize lipid extraction in our yeast strains, and contribute to the LD proteome in the presence and absence of seipin.

Appendix A

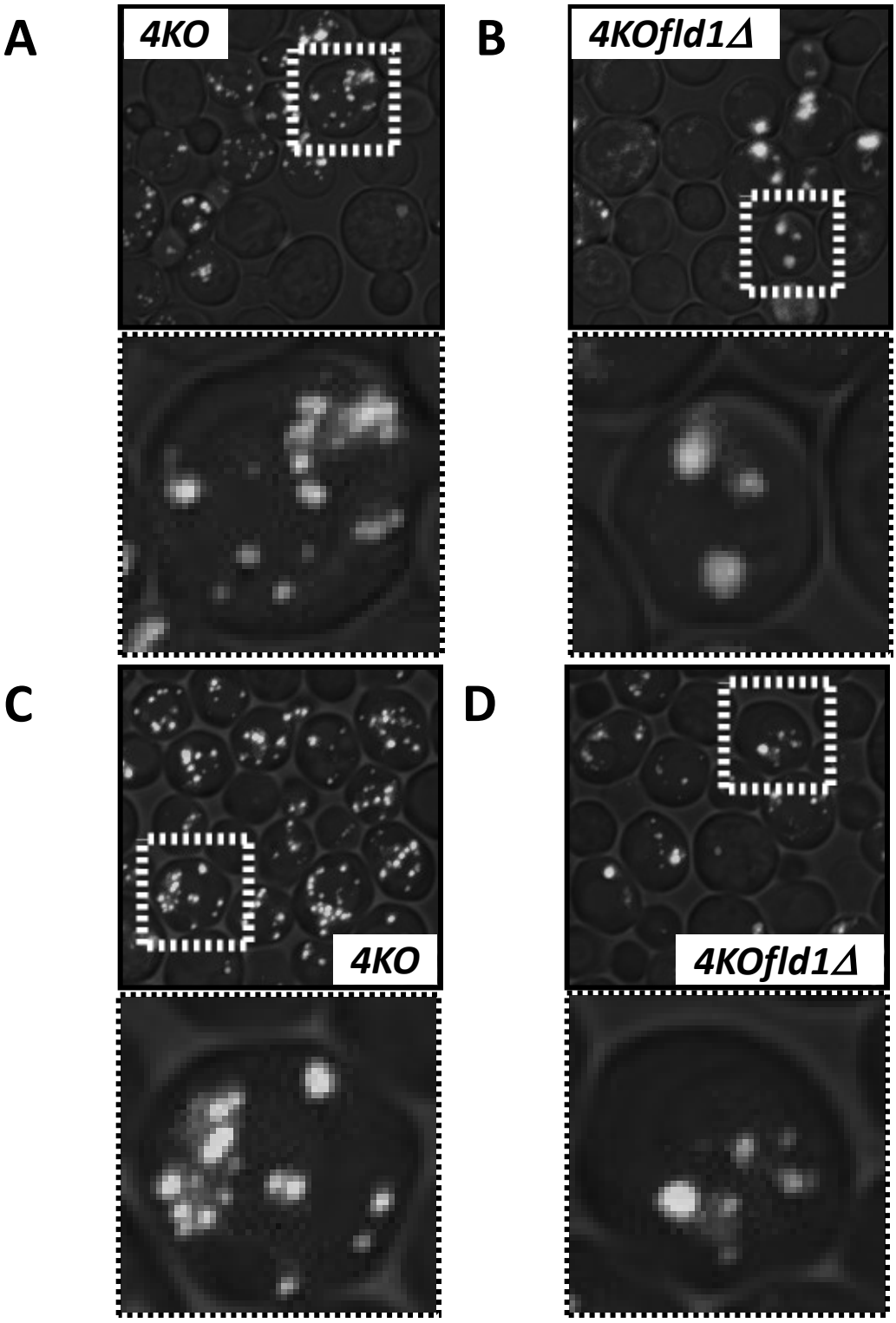
A
4KO
B
4KOfld1Δ
C
4KO
D
4KOfld1Δ

Figure 15. Morphology of *4KO* and *4KOfld1Δ* fluorescent bodies 6 hours after switch to galactose medium. (A) Top: Image from *4KO*, Figure 6, panel A, 6 hr with a striped box indicating where the bottom image was zoomed in from. Bottom: Close-up image of a *4KO* single cell expressing Gal-*DGA1* from the striped box in the top image, also in Figure 6, Panel D. (B) Top: Image from *4KOfld1Δ*, Figure 6, panel A, 6 hr with a striped box indicating where the bottom image was zoomed in from. Bottom: Close-up image of a *4KOfld1Δ* single cell expressing Gal-DGA1 from the striped box in the top image, also in Figure 6, Panel D. (C) Top: Image from *4KO*, Figure 9, panel A, 6 hr with a striped box indicating where the bottom image was zoomed in from. Bottom: Close-up image of a *4KO* single cell expressing Gal-*ARE1* from the striped box in the top image, also in Figure 9, Panel D. (B) Top: Image from *4KOfld1Δ*, Figure 9, panel A, 6 hr with a striped box indicating where the bottom image was zoomed in from. Bottom: Close-up image of a *4KOfld1Δ* single cell expressing Gal-*ARE1* from the striped box in the top image, also in Figure 9, Panel D.

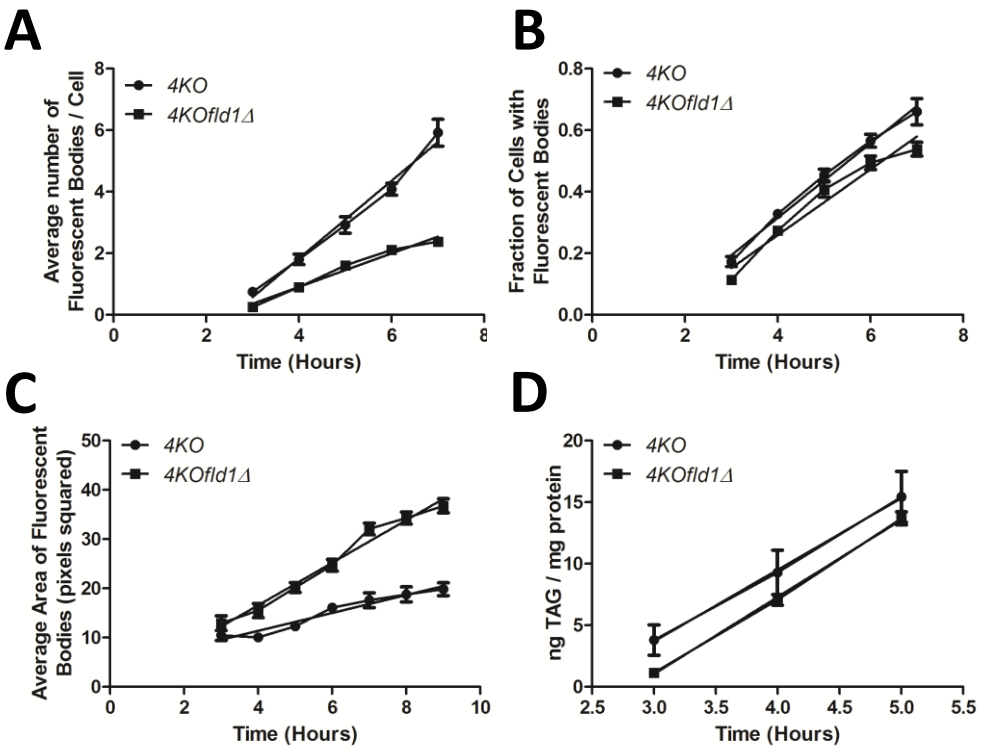

Figure 16. Linear regressions of data from Figure 6 B and C and Figure 7 A.

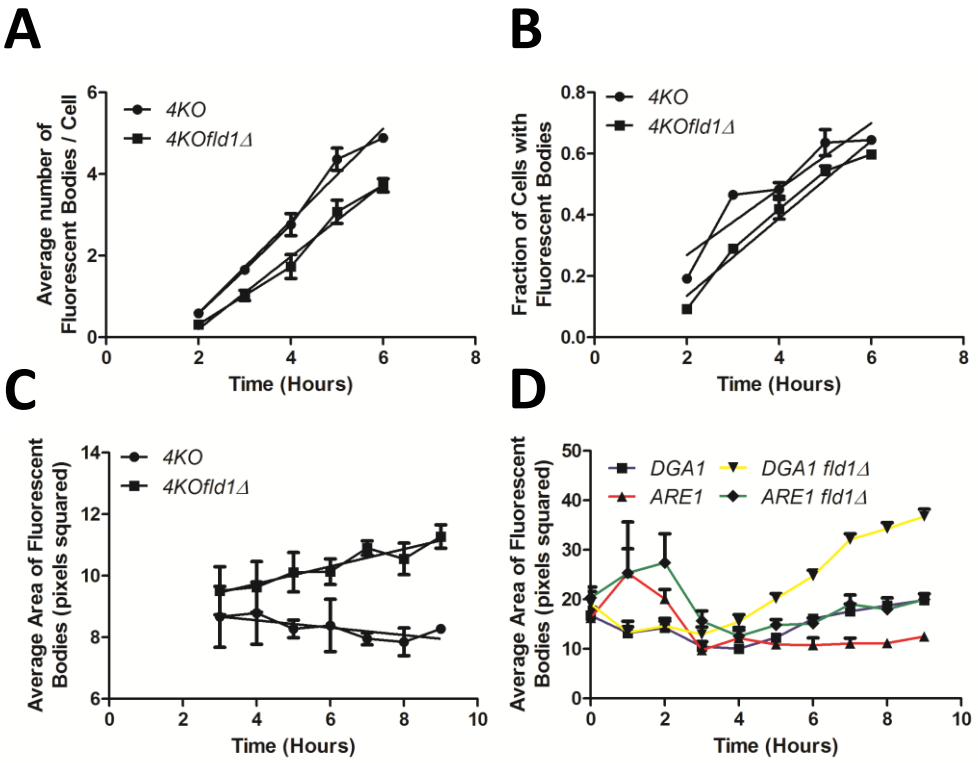

Figure 17. (A-C) Linear regressions of data from Figure 9 B and C. (D) Comparison of the area of FB in strains expressing GAL-*DGA1* compared to those expressing GAL-*ARE1*.

Strain	Genotype	Source or Reference
BY4742 wild type	*MATα his3Δ1 leu2Δ0 lys2Δ0 ura3Δ0*	Open Biosystems (Brachmann *et al.*, 1998)
fld1Δ	BY4742 *fld1Δ::Kan^r*	Open Biosystems (Winzeler *et al.*, 1999)
W303-1A	*MAT*a *leu2-3, 112 trp1-1 can1-100 ura3-1 ade2-1 his3-11,15*	(Veal *et al.*, 2003)
4KO	W303-1A *dga1Δ::URA3 lro1Δ::URA3 are1Δ::HIS3 are2Δ:: LEU2*	Gift from Steve Sturley SCY 2021 (Garbarino *et al.*. 2009)
4KOfld1Δ	*4KO fld1Δ:: hph*	This study; *hph* cassette gift from Ben Tu lab (Goldstein *et al.*, 1999)
seipin-myc13	BY4742 *fld1Δ::FLD1* ORF fused to myc13 followed by *TADH* term and *HIS3*	(Binns *et al.*, 2010)
ire1Δ	BY4742 *ire1Δ::Kan^r*	Open Biosystems (Winzeler *et al.*, 1999)
ire1Δfld1Δ	*ire1Δ fld1Δ::HIS3*	This study
Plasmid	**Description**	**Source or Reference**
pRS314	Yeast centromeric plasmid with *TRP1* marker	(Sikorski & Hieter, 1989)
pRS314-GAL-*DGA1*	pRS314 expressing *DGA1* under control of GAL1-10 promoter and PGK3 terminator	This study
pRS314-GAL-*ARE1*	pRS314 expressing *ARE1* under control of GAL1-10 promoter and PGK3 terminator	This study

References

1. Suzuki, M., Shinohara, Y., Ohsaki, Y. & Fujimoto, T. Lipid droplets: size matters. *Journal of Electron Microscopy* **60**, S101-S116 (2011).
2. Szymanski, K.M. *et al.* The lipodystrophy protein seipin is found at endoplasmic reticulum lipid droplet junctions and is important for droplet morphology. *Proc Natl Acad Sci U S A* **104**, 20890-20895 (2007).
3. Magre, J. *et al.* Identification of the gene altered in Berardinelli-Seip congenital lipodystrophy on chromosome 11q13. *Nat Genet* **28**, 365-370 (2001).
4. Agarwal, A.K. *et al.* Phenotypic and Genetic Heterogeneity in Congenital Generalized Lipodystrophy. *Journal of Clinical Endocrinology & Metabolism* **88**, 4840-4847 (2003).
5. Bonilla, F.A. Development of Population-Based Newborn Screening for Severe Combined Immunodeficiency. *Pediatrics* **118**, S47 (2006).
6. Buckley, R.H. The multiple causes of human SCID. *The Journal of Clinical Investigation* **114**, 1409-1411 (2004).
7. Miller, J. *et al.* HIV lipodystrophy: prevalence, severity and correlates of risk in Australia. *HIV Medicine* **4**, 293-301 (2003).
8. Giralt, M. *et al.* HIV-1 infection alters gene expression in adipose tissue, which contributes to HIV- 1/HAART-associated lipodystrophy. *Antiviral Therapy* **11**, 729-740 (2006).
9. Reeves, W.G., Allen, B.R. & Tattersall, R.B. Insulin-induced lipoatrophy: evidence for an immune pathogenesis. *BMJ* **280** (1980).
10. Kayikcioglu, A., AkyÃ¼rek, M. & Erk, Y.c. Semicircular lipoatrophy after intragluteal injection of benzathine penicillin. *The Journal of Pediatrics* **129**, 166-167 (1996).
11. Andre, P. Post corticosteroid lipo atrophy treated by fat grafting. *Annales de Dermatologie et de Venereologie* **117**, 733-734 (1990).
12. Dahl, P.R., Zalla, M.J. & Winkelmann, R.K. Localized involutional lipoatrophy: A clinicopathologic study of 16 patients. *Journal of the American Academy of Dermatology* **35**, 523-528 (1996).
13. Simha, V. & Garg, A. Phenotypic heterogeneity in body fat distribution in patients with congenital generalized lipodystrophy caused by mutations in the AGPAT2 or seipin genes. *J Clin Endocrinol Metab* **88**, 5433-5437 (2003).
14. Geffner, M.E. & Golde, D.W. Selective Insulin Action on Skin, Ovary, and Heart in Insulin-Resistant States. *Diabetes Care* **11**, 500-505 (1988).

15. Nguyen, T.T., Sheppard, A.M., Kaye, P.L. & Noakes, P.G. IGF-I and insulin activate mitogen-activated protein kinase via the type 1 IGF receptor in mouse embryonic stem cells. *Reproduction* **134**, 41-49 (2007).
16. Antuna-Puente, B. *et al.* Higher Adiponectin Levels in Patients with Berardinelli-Seip Congenital Lipodystrophy due to Seipin as compared with 1-Acylglycerol-3-Phosphate-O-Acyltransferase-2 Deficiency. *J Clin Endocrinol Metab* (2010).
17. Baker, J., Liu, J.-P., Robertson, E.J. & Efstratiadis, A. Role of insulin-like growth factors in embryonic and postnatal growth. *Cell* **75**, 73-82 (1993).
18. Stratikopoulos, E., Szabolcs, M., Dragatsis, I., Klinakis, A. & Efstratiadis, A. The hormonal action of IGF1 in postnatal mouse growth. *Proceedings of the National Academy of Sciences* **105**, 19378-19383 (2008).
19. Woods, K.A. *et al.* Effects of Insulin-Like Growth Factor I (IGF-I) Therapy on Body Composition and Insulin Resistance in IGF-I Gene Deletion. *Journal of Clinical Endocrinology & Metabolism* **85**, 1407-1411 (2000).
20. Liu, J.-m. *et al.* IGF-1 as an early marker for low bone mass or osteoporosis in premenopausal and postmenopausal women. *Journal of Bone and Mineral Metabolism* **26**, 159-164 (2008).
21. Zapf, J., Rinderknecht, E., Humbel, R.E. & Froesch, E.R. Nonsuppressible insulin-like activity (NSILA) from human serum: Recent accomplishments and their physiologic implications. *Metabolism* **27**, 1803-1828 (1978).
22. Van Maldergem, L. *et al.* Genotype-phenotype relationships in Berardinelli-Seip congenital lipodystrophy. *J Med Genet* **39**, 722-733 (2002).
23. Haque, W.A., Shimomura, I., Matsuzawa, Y. & Garg, A. Serum Adiponectin and Leptin Levels in Patients with Lipodystrophies. *Journal of Clinical Endocrinology & Metabolism* **87**, 2395 (2002).
24. Arihara, Z., Sakurai, K., Yamada, S., Murakami, O. & Takahashi, K. Acromegaly with Normal IGF-1 Levels Probably due to Poorly Controlled Diabetes Mellitus. *The Tohoku Journal of Experimental Medicine* **216**, 325-329 (2008).
25. Rommel, C. *et al.* Mediation of IGF-1-induced skeletal myotube hypertrophy by PI(3)K/Akt/mTOR and PI(3)K/Akt/GSK3 pathways. *Nat Cell Biol* **3**, 1009-1013 (2001).
26. Berardinelli, W. AN UNDIAGNOSED ENDOCRINOMETABOLIC SYNDROME: REPORT OF 2 CASES. *Journal of Clinical Endocrinology & Metabolism* **14**, 193-204 (1954).
27. Barbieri, R.L. *et al.* Insulin Stimulates Androgen Accumulation in Incubations of Ovarian Stroma Obtained from Women with

Hyperandrogenism. *Journal of Clinical Endocrinology & Metabolism* **62**, 904-910 (1986).
28. Miehle, K., Stumvoll, M. & Fasshauer, M. [Lipodystrophy: Mechanisms, clinical presentation, therapy]. *Der Internist* **52**, 362-373 (2011).
29. Monajemi, H., Stroes, E., Hegele, R.A. & Fliers, E. Inherited lipodystrophies and the metabolic syndrome. *Clinical Endocrinology* **67**, 479-484 (2007).
30. Agarwal, A.K. & Garg, A. Genetic Basis of Lipodystrophies and Management of Metabolic Complications. *Annual Review of Medicine* **57**, 297-311 (2006).
31. Agarwal, A.K., Barnes, R.I. & Garg, A. Genetic basis of congenital generalized lipodystrophy. *Int J Obes Relat Metab Disord* **28**, 336-339 (2004).
32. Arioglu, E. *et al.* Efficacy and Safety of Troglitazone in the Treatment of Lipodystrophy Syndromes. *Annals of Internal Medicine* **133**, 263-274 (2000).
33. Chong, A.Y., Lupsa, B.C., Cochran, E.K. & Gorden, P. Efficacy of leptin therapy in the different forms of human lipodystrophy. *Diabetologia* **53**, 27-35 (2010).
34. Oral, E.A. *et al.* Leptin-Replacement Therapy for Lipodystrophy. *New England Journal of Medicine* **346**, 570-578 (2002).
35. Nistri, S. *et al.* Beta Blockers for Prevention of Exercise-Induced Left Ventricular Outflow Tract Obstruction in Patients With Hypertrophic Cardiomyopathy. *The American journal of cardiology* (2012).
36. Ball, W. *et al.* Long-Term Survival in Patients With Resting Obstructive Hypertrophic Cardiomyopathy: Comparison of Conservative Versus Invasive Treatment. *J Am Coll Cardiol* **58**, 2313-2321 (2011).
37. Lacovoni, A. *et al.* A contemporary European experience with surgical septal myectomy in hypertrophic cardiomyopathy. *European Heart Journal* (2012).
38. Brady, P.A. Surviving hypertrophic cardiomyopathy: counting the cost of implantable cardioverter defibrillator therapy to prevent sudden death. *Heart* **98**, 97-98 (2012).
39. Fu, M. *et al.* Mutations in Gng3lg and AGPAT2 in Berardinelli-Seip Congenital Lipodystrophy and Brunzell Syndrome: Phenotype Variability Suggests Important Modifier Effects. *Journal of Clinical Endocrinology & Metabolism* **89**, 2916-2922 (2004).
40. Agarwal, A.K. & Garg, A. Seipin: a mysterious protein. *Trends Mol Med* **10**, 440-444 (2004).
41. Rajab, A. *et al.* Fatal Cardiac Arrhythmia and Long-QT Syndrome in a New Form of Congenital Generalized Lipodystrophy with Muscle

Rippling (CGL4) Due to <italic>PTRF-CAVIN</italic> Mutations. *PLoS Genet* **6**, e1000874 (2010).
42. Hayashi, Y.K. *et al.* Human PTRF mutations cause secondary deficiency of caveolins resulting in muscular dystrophy with generalized lipodystrophy. *Journal of Clinical Investigation* **119**, 2623-2633 (2009).
43. Williams, T. & Lisanti, M. The caveolin proteins. *Genome Biology* **5**, 214 (2004).
44. Hill, M.M. *et al.* PTRF-Cavin, a Conserved Cytoplasmic Protein Required for Caveola Formation and Function. *Cell* **132**, 113-124 (2008).
45. Kim, C.A. *et al.* Association of a homozygous nonsense caveolin-1 mutation with Berardinelli-Seip congenital lipodystrophy. *J Clin Endocrinol Metab* **93**, 1129-1134 (2008).
46. Razani, B. *et al.* Caveolin-1-deficient Mice Are Lean, Resistant to Diet-induced Obesity, and Show Hypertriglyceridemia with Adipocyte Abnormalities. *Journal of Biological Chemistry* **277**, 8635-8647 (2002).
47. Shastry, S. *et al.* Congenital generalized lipodystrophy, type 4 (CGL4) associated with myopathy due to novel PTRF mutations. *American Journal of Medical Genetics Part A* **152A**, 2245-2253 (2010).
48. Kim, H., MelÃ©n, K. & von Heijne, G. Topology Models for 37 Saccharomyces cerevisiaeMembrane Proteins Based on C-terminal Reporter Fusions and Predictions. *Journal of Biological Chemistry* **278**, 10208-10213 (2003).
49. Windpassinger, C. *et al.* Heterozygous missense mutations in BSCL2 are associated with distal hereditary motor neuropathy and Silver syndrome. *Nat Genet* **36**, 271-276 (2004).
50. Lundin, C. *et al.* Membrane topology of the human seipin protein. *FEBS Lett* **580**, 2281-2284 (2006).
51. Cartwright, B.R. & Goodman, J.M. Seipin: from human disease to molecular mechanism. *Journal of Lipid Research* **53**, 1042-1055 (2012).
52. Ito, D., Fujisawa, T., Iida, H. & Suzuki, N. Characterization of seipin/BSCL2, a protein associated with spastic paraplegia 17. *Neurobiol Dis* **31**, 266-277 (2008).
53. Chen, W. *et al.* The human lipodystrophy gene product Berardinelli-Seip congenital lipodystrophy 2/seipin plays a key role in adipocyte differentiation. *Endocrinology* **150**, 4552-4561 (2009).
54. Payne, V.A. *et al.* The human lipodystrophy gene BSCL2/seipin may be essential for normal adipocyte differentiation. *Diabetes* **57**, 2055-2060 (2008).
55. Tian, Y. *et al.* Tissue-Autonomous Function of Drosophila Seipin in Preventing Ectopic Lipid Droplet Formation. *PLoS Genet* **7**, e1001364 (2011).

56. Luigetti, M. *et al.* SEIPIN S90L Mutation in an Italian family with CMT2/dHMN and pyramidal signs. *Muscle & Nerve* **42**, 448-451 (2010).
57. Ito, D. & Suzuki, N. Molecular pathogenesis of seipin/BSCL2-related motor neuron diseases. *Ann Neurol* **61**, 237-250 (2007).
58. Ito, D. & Suzuki, N. Seipinopathy: a novel endoplasmic reticulum stress-associated disease. *Brain* **132**, 8-15 (2009).
59. Ito, D., Yagi, T., Ikawa, M. & Suzuki, N. Characterization of inclusion bodies with cytoprotective properties formed by seipinopathy-linked mutant seipin. *Human Molecular Genetics* **21**, 635-646 (2012).
60. Fei, W. *et al.* Fld1p, a functional homologue of human seipin, regulates the size of lipid droplets in yeast. *J Cell Biol* **180**, 473-482 (2008).
61. Boutet, E. *et al.* Seipin deficiency alters fatty acid Delta9 desaturation and lipid droplet formation in Berardinelli-Seip congenital lipodystrophy. *Biochimie* **91**, 796-803 (2009).
62. Fei, W. *et al.* A Role for Phosphatidic Acid in the Formation of Supersized Lipid Droplets. *PLoS Genet* **7**, e1002201 (2011).
63. Wolinski, H., Kolb, D., Hermann, S., Koning, R.I. & Kohlwein, S.D. A role for seipin in lipid droplet dynamics and inheritance in yeast. *Journal of Cell Science* **124**, 3894-3904 (2011).
64. Chen, W. *et al.* Berardinelli-Seip Congenital Lipodystrophy 2/Seipin Is a Cell-Autonomous Regulator of Lipolysis Essential for Adipocyte Differentiation. *Molecular and Cellular Biology* **32**, 1099-1111 (2012).
65. Cui, X. *et al.* Seipin ablation in mice results in severe generalized lipodystrophy. *Human Molecular Genetics* **20**, 3022-3030 (2011).
66. Adeyo, O. *et al.* The yeast lipin orthologue Pah1p is important for biogenesis of lipid droplets. *J Cell Biol* **192**, 1043-1055 (2011).
67. Ghaemmaghami, S. *et al.* Global analysis of protein expression in yeast. *Nature* **425**, 737-741 (2003).
68. Binns, D., Lee, S., Hilton, C.L., Jiang, Q.X. & Goodman, J.M. Seipin is a discrete homooligomer. *Biochemistry* **49**, 10747-10755 (2010).
69. Babitzke, P., Bear, D.G. & Yanofsky, C. TRAP, the trp RNA-binding attenuation protein of Bacillus subtilis, is a toroid-shaped molecule that binds transcripts containing GAG or UAG repeats separated by two nucleotides. *Proceedings of the National Academy of Sciences* **92**, 7916-7920 (1995).
70. Melville, M.W., McClellan, A.J., Meyer, A.S., Darveau, A. & Frydman, J. The Hsp70 and TRiC/CCT Chaperone Systems Cooperate In Vivo To Assemble the Von Hippel-Lindau Tumor Suppressor Complex. *Molecular and Cellular Biology* **23**, 3141-3151 (2003).
71. Henry, S.A., Patton-Vogt, J.L. & Kivie, M. Genetic Regulation of Phospholipid Metabolism: Yeast as a Model Eukaryote, in *Progress in*

Nucleic Acid Research and Molecular Biology, Vol. Volume 61 133-179 (Academic Press, 1998).
72. Carman, G.M. & Henry, S.A. Phospholipid biosynthesis in the yeast Saccharomyces cerevisiae and interrelationship with other metabolic processes. *Progress in Lipid Research* **38**, 361-399 (1999).
73. Fei, W. *et al.* Molecular characterization of seipin and its mutants: implications for seipin in triacylglycerol synthesis. *Journal of Lipid Research* **52**, 2136-2147 (2011).
74. Cui, X. *et al.* Overexpression of a short human seipin/BSCL2 isoform in mouse adipose tissue results in mild lipodystrophy. *American Journal of Physiology - Endocrinology And Metabolism* **302**, E705-E713 (2012).
75. Urs, S., Harrington, A., Liaw, L. & Small, D. Selective expression of an aP2/Fatty Acid Binding Protein4-Cre transgene in non-adipogenic tissues during embryonic development. *Transgenic Research* **15**, 647-653 (2006).
76. Victoria, B. *et al.* Reduced adipogenic gene expression in fibroblasts from a patient with type 2 congenital generalized lipodystrophy. *Diabetic Medicine* **27**, 1178-1187 (2010).
77. Kuerschner, L., Moessinger, C. & Thiele, C. Imaging of lipid biosynthesis: how a neutral lipid enters lipid droplets. *Traffic* **9**, 338-352 (2008).
78. Sorger, D. & Daum, G.n. Synthesis of Triacylglycerols by the Acyl-Coenzyme A:Diacyl-Glycerol Acyltransferase Dga1p in Lipid Particles of the Yeast Saccharomyces cerevisiae. *Journal of Bacteriology* **184**, 519-524 (2002).
79. Zehmer, J.K. *et al.* Targeting sequences of UBXD8 and AAM-B reveal that the ER has a direct role in the emergence and regression of lipid droplets. *Journal of Cell Science* **122**, 3694-3702 (2009).
80. Welte, M.A. Fat on the move: intracellular motion of lipid droplets. *Biochemistry Society Transactions* **37**, 991-996 (2009).
81. Tauchi-Sato, K., Ozeki, S., Houjou, T., Taguchi, R. & Fujimoto, T. The Surface of Lipid Droplets Is a Phospholipid Monolayer with a Unique Fatty Acid Composition. *Journal of Biological Chemistry* **277**, 44507-44512 (2002).
82. Zehmer, J.K. *et al.* A role for lipid droplets in inter-membrane lipid traffic. *PROTEOMICS* **9**, 914-921 (2009).
83. Kalantari, F., Bergeron, J.J.M. & Nilsson, T. Biogenesis of lipid droplets: how cells get fatter. *Molecular Membrane Biology* **27**, 462-468 (2010).
84. Gorrissen, H. *et al.* Deuterium magnetic resonance of selectively deuterated cholesteryl-esters in dipalmitoyl phosphatidylcholine dispersions. *Biochim Biophys Acta* **644**, 266-272 (1981).

85. Gorrissen, H., Tulloch, A.P. & Cushley, R.J. Deuterium magnetic resonance of triacylglycerols in phospholipid bilayers. *Chem Phys Lipids* **31**, 245-255 (1982).
86. Khandelia, H., Duelund, L., Pakkanen, K.I. & Ipsen, J.H. Triglyceride Blisters in Lipid Bilayers: Implications for Lipid Droplet Biogenesis and the Mobile Lipid Signal in Cancer Cell Membranes. *PLoS ONE* **5**, e12811 (2010).
87. Lemberg, M.K., Bland, F.A., Weihofen, A., Braud, V.M. & Martoglio, B. Intramembrane Proteolysis of Signal Peptides: An Essential Step in the Generation of HLA-E Epitopes. *The Journal of Immunology* **167**, 6441-6446 (2001).
88. Goodman, J.M. The Gregarious Lipid Droplet. *Journal of Biological Chemistry* **283**, 28005-28009 (2008).
89. Jacquier, N. *et al.* Lipid droplets are functionally connected to the endoplasmic reticulum in Saccharomyces cerevisiae. *Journal of Cell Science* **124**, 2424-2437 (2011).
90. Walther, T.C. & Farese Jr, R.V. The life of lipid droplets. *Biochimica et Biophysica Acta (BBA) - Molecular and Cell Biology of Lipids* **1791**, 459-466 (2009).
91. Robenek, H. *et al.* Topography of Lipid Droplet-Associated Proteins: Insights from Freeze-Fracture Replica Immunogold Labeling. *Journal of Lipids* **2011** (2010).
92. Robenek, H. *et al.* Adipophilin-enriched domains in the ER membrane are sites of lipid droplet biogenesis. *J Cell Sci* **119**, 4215-4224 (2006).
93. Ozeki, S. *et al.* Rab18 localizes to lipid droplets and induces their close apposition to the endoplasmic reticulum-derived membrane. *Journal of Cell Science* **118**, 2601-2611 (2005).
94. Beller, M. *et al.* COPI Complex Is a Regulator of Lipid Homeostasis. *Plos Biology* **6**, 2530-2549 (2008).
95. Soni, K.G. *et al.* Coatomer-dependent protein delivery to lipid droplets. *Journal of Cell Science* **122**, 1834-1841 (2009).
96. Nakamura, N., Banno, Y. & Tamiya-Koizumi, K. Arf1-dependent PLD1 is localized to oleic acid-induced lipid droplets in NIH3T3 cells. *Biochemical and Biophysical Research Communications* **335**, 117-123 (2005).
97. Guo, Y. *et al.* Functional genomic screen reveals genes involved in lipid-droplet formation and utilization. *Nature* **453**, 657-661 (2008).
98. Dvorak, A.M., Morgan, E.S. & Weller, P.F. RNA is closely associated with human mast cell lipid bodies. *Histol Histopathol* **18**, 943-968 (2003).
99. Wolinski, H., Bredies, K., Kohlwein, S.D., Gilbert Di, P. & Markus, R.W. Chapter 16 - Quantitative Imaging of Lipid Metabolism in Yeast: From

4D Analysis to High Content Screens of Mutant Libraries, in *Methods in Cell Biology*, Vol. Volume 108 345-365 (Academic Press, 2012).
100. Hundová, Z. & Fencl, Z. Toxic effects of fatty acids on yeast cells: Dependence of inhibitory effects on fatty acid concentration. *Biotechnology and Bioengineering* **19**, 1623-1641 (1977).
101. Wright, R. Transmission electron microscopy of yeast. *Microscopy Research and Technique* **51**, 496-510 (2000).
102. Binns, D. *et al.* An intimate collaboration between peroxisomes and lipid bodies. *The Journal of Cell Biology* **173**, 719-731 (2006).
103. Bligh, E.G. & Dyer, W.J. A rapid method of total lipid extraction and purification. *Can J Biochem Physiol* **37**, 911-917 (1959).
104. Leber, R., Zinser, E., Paltauf, F., Daum, G. & Zellnig, G. Characterization of lipid particles of the yeast, Saccharomyces cerevisiae. *Yeast* **10**, 1421-1428 (1994).
105. Athenstaedt, K., Zweytick, D., Jandrositz, A., Kohlwein, S.D. & Daum, G.n. Identification and Characterization of Major Lipid Particle Proteins of the Yeast Saccharomyces cerevisiae. *Journal of Bacteriology* **181**, 6441-6448 (1999).
106. Lowry, O.H., Rosebrough, N.J., Farr, A.L. & Randall, R.J. PROTEIN MEASUREMENT WITH THE FOLIN PHENOL REAGENT. *Journal of Biological Chemistry* **193**, 265-275 (1951).
107. Laemmli, U.K. Cleavage of Structural Proteins during the Assembly of the Head of Bacteriophage T4. *Nature* **227**, 680-685 (1970).
108. Wray, W., Boulikas, T., Wray, V.P. & Hancock, R. Silver staining of proteins in polyacrylamide gels. *Analytical Biochemistry* **118**, 197-203 (1981).
109. Shimoni, Y., Schekman, R. & Christine Guthrie, G.R.F. Vesicle budding from endoplasmic reticulum, in *Methods in Enzymology*, Vol. Volume 351 258-278 (Academic Press, 2002).
110. Tanford, C., Nozaki, Y. & Rohde, M.F. Size and shape of globular micelles formed in aqueous solution by n-alkyl polyoxyethylene ethers. *The Journal of Physical Chemistry* **81**, 1555-1560 (1977).
111. Friesen, R.H.E., Knol, J. & Poolman, B. Quaternary structure of the lactose transport protein of Streptococcus thermophilus in the detergent-solubilized and membrane-reconstituted state. *Journal of Biological Chemistry* **275**, 40658 (2000).
112. Aragon, C., Lopez-Corcuera, B. & Susan, G.A. [1] Purification, hydrodynamic properties, and glycosylation analysis of glycine transporters, in *Methods in Enzymology*, Vol. Volume 296 3-17 (Academic Press, 1998).

113. Tanford, C. & Reynolds, J.A. Characterization of membrane proteins in detergent solutions. *Biochimica et Biophysica Acta (BBA) - Reviews on Biomembranes* **457**, 133-170 (1976).
114. Sandager, L. *et al.* Storage Lipid Synthesis Is Non-essential in Yeast. *Journal of Biological Chemistry* **277**, 6478-6482 (2002).
115. Klis, F.M., Boorsma, A. & De Groot, P.W.J. Cell wall construction in Saccharomyces cerevisiae. *Yeast* **23**, 185-202 (2006).
116. Schneiter, R., Daum, G. & Xiao, W. Analysis of Yeast Lipids Yeast Protocol, in, Vol. 313. (ed. J.M. Walker) 75-84 (Humana Press, 2006).
117. Folch, J., Lees, M. & Stanley, G.H.S. A SIMPLE METHOD FOR THE ISOLATION AND PURIFICATION OF TOTAL LIPIDES FROM ANIMAL TISSUES. *Journal of Biological Chemistry* **226**, 497-509 (1957).
118. Paar, M. *et al.* Remodeling Of lipid droplets during lipolysis and growth in adipocytes. *Journal of Biological Chemistry*.
119. Brown, J.M. *et al.* CGI-58 facilitates the mobilization of cytoplasmic triglyceride for lipoprotein secretion in hepatoma cells. *Journal of Lipid Research* **48**, 2295-2305 (2007).
120. Du, W. & Ayscough, K.R. Methyl Beta-cyclodextrin reduces accumulation of reactive oxygen species and cell death in yeast. *Free Radical Biology and Medicine* **46**, 1478-1487 (2009).